Epoxidation Reaction of Soybean Oil: Experimental Study and Comprehensive Kinetic Modeling

*Gustavo V. Olivieri, Jacyr V. de Quadros Jr., Reinaldo Giudici**

Universidade de São Paulo, Escola Politécnica, Department of Chemical Engineering, Av. Prof. Luciano Gualberto, Travessa 3, No. 380, 05508-010, São Paulo, Brazil

Keywords: Epoxidation reaction; Epoxidized soybean oil; Kinetic modeling; Apparent kinematic viscosity.

ABSTRACT

Epoxidized soybean oil (ESO) has been considered to be a green alternative to replace petroleum-based substances as a plasticizer for polyvinyl chloride (PVC). ESO is usually produced in a biphasic reaction system, in which hydrogen peroxide reacts with a carboxylic acid in the aqueous phase to generate an organic peracid that migrates to the organic phase and reacts with the soybean oil to produce ESO. The present study includes experimental data obtained in a previous work, to prepare ESO from soybean oil in a 4 h reaction time under different conditions, with single addition of the reactants and in the absence of catalysts. The paper also proposes a more robust model to predict the effects related to the hydrogen peroxide and formic acid amounts, the stirring speed, the thermostatic bath temperature and the apparent kinematic viscosity of the system. The experimental results were used to fit a kinetic model for this system,

including the heat and mass transfer effects and the undesired reactions. Additionally, the model included a satisfactory prediction of the changes in the apparent kinematic viscosity of the system, significantly improving the description of the heat transfer effects.

1. Introduction

One of the current challenges, common in different fields of the chemical industry, is the search for substances and/or technologies that follow the Green Chemistry principles and are competitive from an economical point of view. Within the chemical reactions sphere, several studies have been performed to analyze the replacement of nonrenewable and/or highly toxic substances with renewable ones, or, at least, less impacting for the environment. In particular, epoxidized soybean oil (ESO) has been considered to be a promising candidate to replace phthalates as a plasticizer for polyvinyl chloride (PVC), since ESO is obtained from a renewable source (soybean oil) and is biodegradable, in contrast to the phthalates, which are petroleum-based substances with health implications [1–5].

Actually, the addition of ESO to PVC as a primary plasticizer provides low efficiency of plasticization, due to the lower compatibility between these compounds, limiting the application of ESO to that of a secondary plasticizer for PVC [3]. Nevertheless, a synergistic effect of ESO with cardanol, a primary plasticizer also obtained from renewable sources, has been analyzed by Lee et al. [3]. An interesting alternative would be the functionalization of ESO in order to improve the compatibility between ESO and PVC [6]. Another alternative is the production of primary plasticizers derived from ESO [4,5].

In addition to the main studies involving ESO as a plasticizer for PVC, several interesting applications of ESO have been developed. Some examples have been highlighted: Kong et al. [7]

verified the viability of using the ESO as a plasticizer for poly(latic acid) (PLA), in addition to a synergistic effect with a functional eggshell as a nucleating agent; Ciannamea and Ruseckaite [8] and Lee et al. [9] studied the use of ESO as a pressure-sensitive adhesive, after a curing process; Xu et al. [10] developed cellulose aerogels with grafted ESO, aiming at the absorption of oil from oil spills in the ocean.

The most commonly applied method to obtain ESO is based on the Prileschajew reaction, in which soybean oil reacts with an organic peracid, usually performic or peracetic acid. Since the organic peracids are unstable, it is advisable to produce them *in situ* from the reaction of hydrogen peroxide with the corresponding carboxylic acid. Formic acid is preferred over acetic acid due to its higher reactivity, eliminating the need for catalysts such as sulphuric or phosphoric acid [11–13]. Due to solubility issues, this reaction system is biphasic, with the peracid synthesis occurring in the aqueous phase and the Prileschajew reaction taking place in the organic phase, with mass transfer of the carboxylic acid and the peracid between phases.

Nevertheless, some undesired reactions can also occur in this biphasic system: the decomposition of hydrogen peroxide [14–16] and the peracid and the ring opening reactions of ESO. Santacesaria et al. [17] concluded that the decomposition of hydrogen peroxide is relevant only when the pH is alkaline and Di Serio et al. [18] mention that this reaction only becomes important at temperatures above 90 ºC. Since these conditions do not apply to the present work, the decomposition reaction of hydrogen peroxide was considered to be negligible. Additionally, the ESO ring-opening reactions were extensively studied by Campanella and Baltanás [12,19–21] and Cai et al. [22], who indicated that these reactions occur in the intermediate phase (or interphase) of the system and are influenced by the pH.

Figure 1 shows a schematic summary of the entire reaction system, using formic acid to produce performic acid.

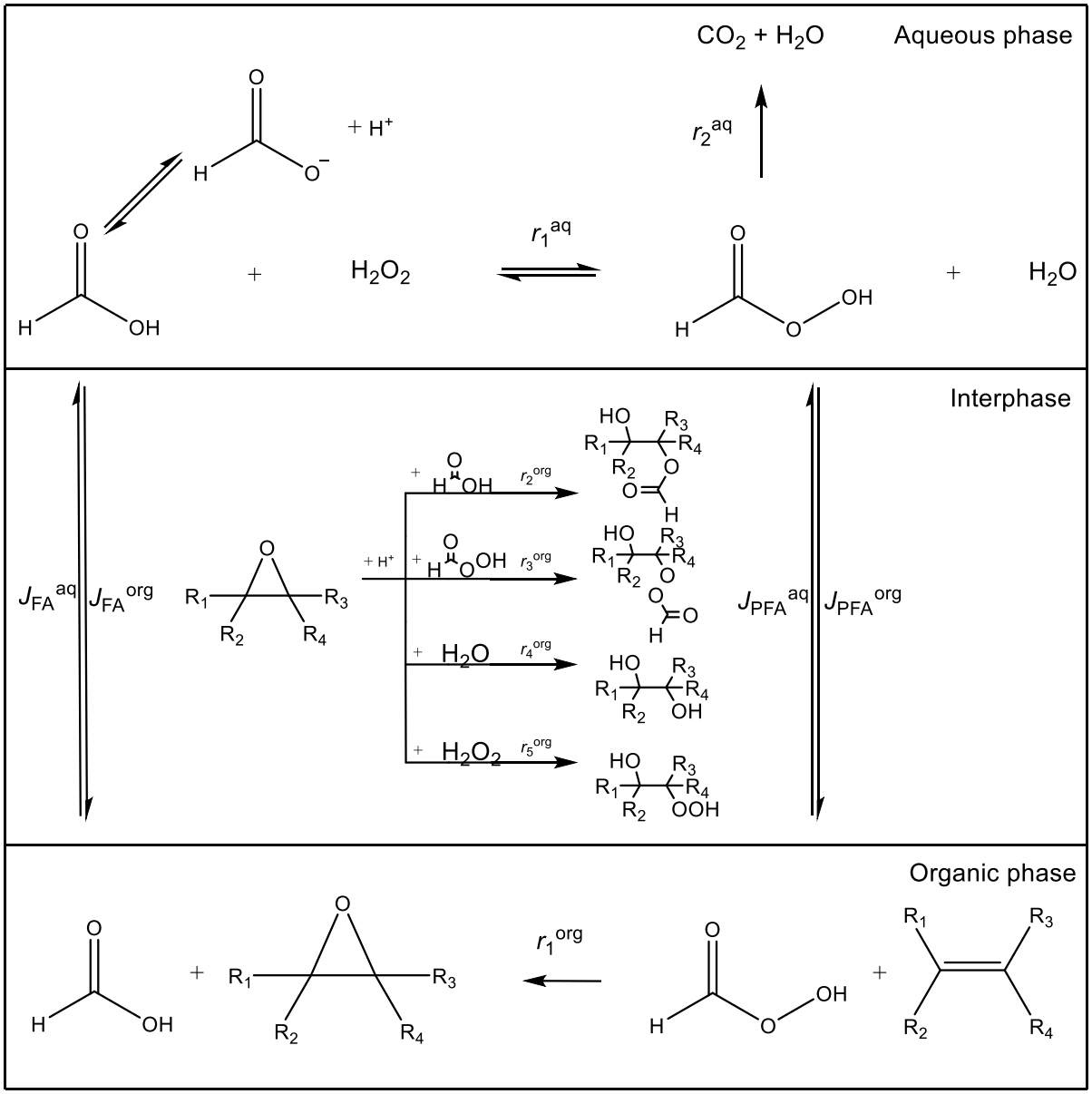

Figure 1. Schematic representation of the reaction system to produce epoxidized soybean oil.

Several authors have proposed kinetic models in order to represent the reaction system for performing the epoxidation of oils and derivatives. Wisniak and Navarrete [23] developed a kinetic

model to describe the main reactions for a homogeneous system for the epoxidation of anchovy oil. Chou and Chang [24] used a similar approach, i.e., lacking information on mass transfer effects, but considering a derivative of vegetable oils (oleic acid). This model was improved to a biphasic system by Rangarajan et al. [25], including the description of the mass transfer effects; these authors also started a description of the ring opening reactions of ESO. Santacesaria et al. [26] described the temperature dependence of the mass transfer coefficients and distinguished the dependence of the kinetics of the epoxidation reaction on the number of unsaturations of the oil (monoene, diene or triene). Wu et al. [27] included the effect of the interfacial area and the pH on the kinetics of the ring opening reactions. Di Serio et al. [18] proposed a kinetic model for a liquid-liquid-solid system, considering a resin as heterogeneous catalyst. Casson Moreno et al. [28] developed a model for a fed-batch system with the aim of evaluating the safest operational conditions and avoid the loss of thermal control (runaway) of the reactor. Wu et al. [29] included an estimate of the interfacial area in the mass transfer equations of the model, after the experimental measurement of the Sauter mean diameter (D_{32}) related to the drops of the dispersed phase (aqueous phase).

The determination of the kinetic parameters for this reaction system has been performed by several authors using different approaches. The majority of these studies determined the kinetic parameters based on the composition of the products in an isothermal approach. This can be exemplified by Cai et al. [30], where the authors estimated the composition of the products based on a chromatographic study. Santacesaria et al. [26] and Zheng et al. [31] used another approach, based on the inclusion of calorimetric terms in the model, i.e., considering the variation of the system temperature.

Aiming at the minimization of the effects of the ring opening reactions, several studies presented promising results after the inclusion of selective catalysts in the reaction system [6,18,32–36], although this might not be economically and/or environmentally advantageous. An alternative to the use of catalysts would be the selection of proper reaction conditions for the system, such as an appropriate temperature control.

The high exothermicity of the epoxidation reaction (with reaction enthalpy estimated as -175 $kJ \cdot mol^{-1}$ [37]) cautions about the thermal effects derived from this reaction system and avoid thermal runaway accident, i.e. the severe increase in temperature that can benefit undesired reactions and even lead to explosions. Nevertheless, the literature encompasses several studies focused on these thermal effects related to the epoxidation of vegetable oils [28,38–42]. Particularly, Cortese et al. [43] proposed to conduct the reaction at higher temperatures than usual, which surpass 100 ºC, by the use of microreactors, which considerably decreases the residence time of the reaction media.

The viability of a single addition of the main components, without the inclusion of catalysts, was studied in a previous project in our Department [44]. This experimental study investigated the reaction system under different conditions in a batch reactor, focusing on the temperature increase due to the single addition of the components and excluding the use of catalysts. The achievement of a thermally safe environment provided conditions to start a deeper study related to the single addition of the components.

Based on this work, the purpose of the present work is to use the experimental data to fit a more robust kinetic model for this system based on a calorimetric approach, supported by data available in the literature and including the heat and mass transfer effects, the undesired reactions and the effect of the apparent viscosity of the system.

2. Methodology

Soybean oil (Bunge, Brazil, with an iodine index of 129), formic acid 85 wt% (Calgon) and hydrogen peroxide 60 wt% (Peróxidos do Brasil) were used without further purification.

The experiments were carried out in a 500 mL glass reactor with controlled stirring, immersed in a 20 L, highly agitated, thermostatic bath with a temperature control of the water within ± 2 ºC. The temperatures of the reaction mixture and the cooling bath were measured with two thermocouples and registered through a data acquisition system. The stirrer employed (IkaLabortechnik, RW20DZM) had accurate speed control and was equipped with a stainless steel mixing paddle of 45 mm diameter.

The experimental tests 01-16, with values specified in Table 1, were performed based on a 2^k factorial planning, with $k = 4$, in which the factors analyzed were: the weight of the formic acid solution (m_{FAS}), the weight of the hydrogen peroxide solution (m_{HPS}), the stirring speed (N) and the temperature of the thermostatic bath (T_b). Here, it can be highlighted that all the tests from the factorial planning (tests 01-16) were performed using a single addition of the hydrogen peroxide solution.

Table 1. Conditions for the tested experiments: stirring speed (N), weight of the formic acid solution (m_{FAS}), weight of the hydrogen peroxide solution (m_{HPS}), temperature of the thermostatic bath (T_b) and number of partitioned additions of the hydrogen peroxide solution.

Test	N / rpm	m_{FAS} / g	m_{HPS} / g	T_b / ºC	Number of

					additions
01	1000	20	100	60	1
02	1000	20	100	40	1
03	1000	20	80	60	1
04	1000	20	80	40	1
05	1000	10	100	60	1
06	1000	10	100	40	1
07	1000	10	80	60	1
08	1000	10	80	40	1
09	500	20	100	60	1
10	500	20	100	40	1
11	500	20	80	60	1
12	500	20	80	40	1
13	500	10	100	60	1
14	500	10	100	40	1
15	500	10	80	60	1
16	500	10	80	40	1
17	400	15	100	60	1
18	400	15	100	60	2
19	400	15	100	60	3
20	400	15	100	60	5
21	400	15	100	60	10
22	400	15	100	60	20
23	500	15	100	60	1
24	700	15	100	60	1
25	1000	15	100	60	1

For the tests 01-16, a constant weight of soybean oil (m_{DB} = 250 g, in which the subscript DB refers to the double bonds of the soybean oil) and the formic acid solution were weighed, added to the reactor and stirred until thermal equilibrium with the thermostatic bath was reached. The appropriate amount of hydrogen peroxide solution was weighted and added to the reactor during an approximate interval of 30-120 s. In parallel with the onset of the addition of hydrogen peroxide, the data acquisition system for the temperature of the reaction medium was turned on. The reaction proceeded for 4 h until the interruption of the stirring. The resulting mixture was transferred to a decantation flask for 24 h. Then, the organic phase was separated and heated on a 120 ºC hot plate until it became translucent with no acid odor. Lastly, the oxirane index and the iodine index of the organic phase were measured with the standardized titration methods ASTM D 1652/AOCS Cd 9-57 and AOCS Cd 1-25, respectively.

The reactor was immersed in a thermostat-controlled bath with 20 L of water, recirculating at 15 L/min, to ensure that the bath temperature would not have any significant variation during the experiments.

The experimental tests 17-22 were performed by a similar procedure, also with m_{DB} = 250 g, but differing in the number of partitioned additions of m_{HPS} to the reactor during an interval of 30-120 s. The temperature profiles resulting from these tests were already presented in our previous study [44], in order to verify the viability of conducting the reaction based on a single addition of the hydrogen peroxide solution. In the present study, the temperature profiles of tests 17-22 were used for validation of the kinetic modeling and will be presented in the corresponding section.

Moreover, test 17 encompassed a periodical collection of 5 mL samples of the reaction system with cold water, to ensure the interruption of the reaction. After submitting the samples to the

same purification procedure described above, the oxirane and iodine indexes for test 17 were measured, in order to generate profiles for these properties.

The procedure for the epoxidation reaction of experimental tests 23-25 was similar to tests 01-16, with m_{DB} = 250 g and a single addition of m_{HPS}. For these tests, the apparent kinematic viscosity of the system was periodically estimated using a very simple capillary viscometer, formed by a glass tube inserted into the reactor. The tube has an internal diameter of 3 mm, with a reduction to 1.5 mm close to the extremity inserted in the reactor, and two marking points. Samples of the reaction system were periodically suctioned inside the tube until it was filled above the two marking points. Then, the time required for the sample to flow between the two marking points back into the reactor was measured. Figure 2 shows a schematic of this apparatus. The *in situ* measurements of the apparent viscosity (based on the principles of Ostwald and Ubbehlode capillary tube viscometers) allowed fast measurements, avoiding significant deviations from the system conditions (temperature, droplet size, composition).

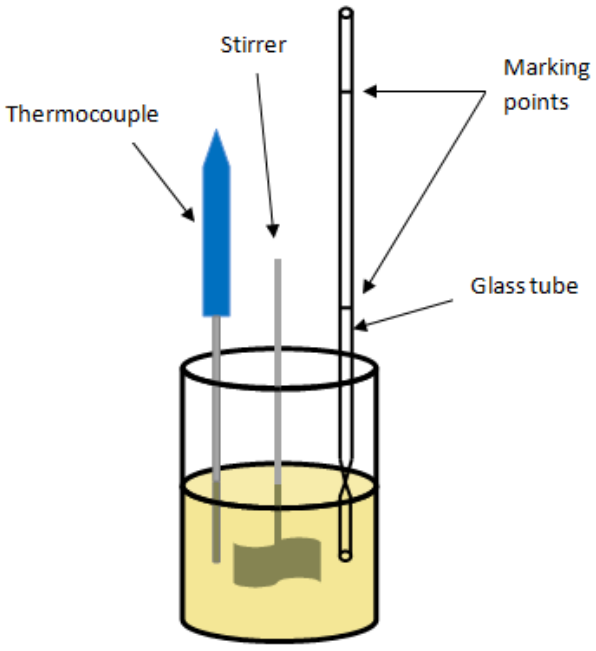

Figure 2. Apparatus for the apparent kinematic viscosity measurements.

Similarly to other capillary viscometers, the measured flow time is directly proportional to the kinematic viscosity of the fluid. In order to estimate the conversion factor between these two properties and evaluate the viability and accuracy of the procedure, the same experiment was performed for pure soybean oil and pure ESO at different temperatures. The flow time was measured in triplicate for each temperature, in which an average value was determined. The kinematic viscosity of soybean oil was reported in the literature [45] and the kinematic viscosity of ESO was measured using a Brookfield viscometer. The relation between the kinematic viscosities and the corresponding average flow times for pure soybean oil and ESO can be observed in Figure 3, which led to an average conversion factor of 1.43×10^{-5} $m^2 \cdot s^{-2}$.

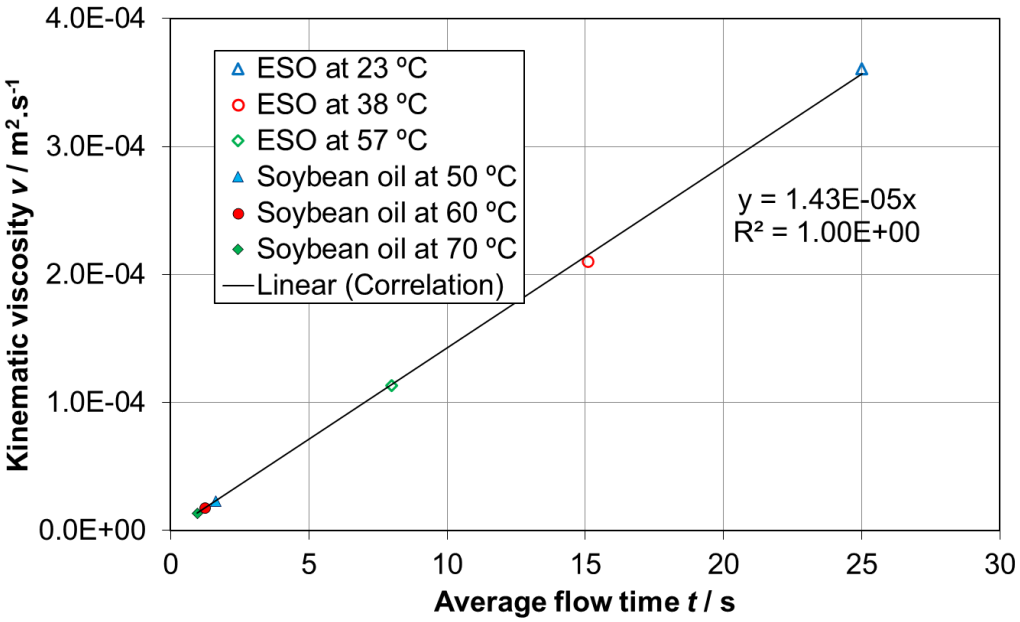

Figure 3. Correlation between the kinematic viscosity (measured in a Brookfield viscosimeter) and the average flow time for pure soybean oil and epoxidized soybean oil measured with the apparatus shown in Figure 2, at different temperatures.

To sum up, the main objective of performing tests 01-16 was the analysis of 4 variables, based on a 2^k factorial planning, measuring temperature profiles and the final values of the iodine and oxirane indexes. Tests 17-22 were performed and presented in our previous study with the aim of verifying the viability of a single addition of all reactants; the temperature profiles concerning these tests will be replicated here for validation of the proposed kinetic model. The periodical collection of samples for Test 17 also enabled the determination of profiles for the iodine and oxirane indexes. Lastly, the objective of tests 23-25 was the determination of a profile for the apparent kinematic viscosity of the system for different values of the stirring speed.

3. Results and discussion

3.1. Experimental results

According to the values specified in Table 1, the reaction system temperatures were measured and the corresponding temperature profiles are presented in Figure 4. Here it is important to emphasize that, despite the presence of a biphasic system, these values of temperature are assumed to be the same for both phases and the interphase, i.e., thermal equilibrium was assumed for the system at each instant.

The results for the iodine index (*II*) and oxirane index (*OI*) for the tests 01-16, at the end of the reaction, as well as the maximum temperature values (T_{max}), are presented in Table 2, jointly with the double bond conversion, the oxirane yield and the selectivity.

The double bond conversion (X) was calculated from the II results, according to Eq. (1), where II_0 represents the iodine index of the pure soybean oil.

$$X = 100(1 - II/II_0) \tag{1}$$

The oxirane yield (Y) was determined from Eq. (2), after the OI measurements, in relation to the theoretical oxirane index (OI_t)

$$Y = 100(OI/OI_t) \tag{2}$$

in which OI_t was determined from Eq. (3), where M is the molar mass.

$$OI_t = 100M_O\left(II_0/M_{I_2}\right)/\left[100 + M_O\left(II_0/M_{I_2}\right)\right] = 7.52\% \tag{3}$$

The selectivity (S) was determined with the relation presented in Eq. (4).

$$S = Y/X \tag{4}$$

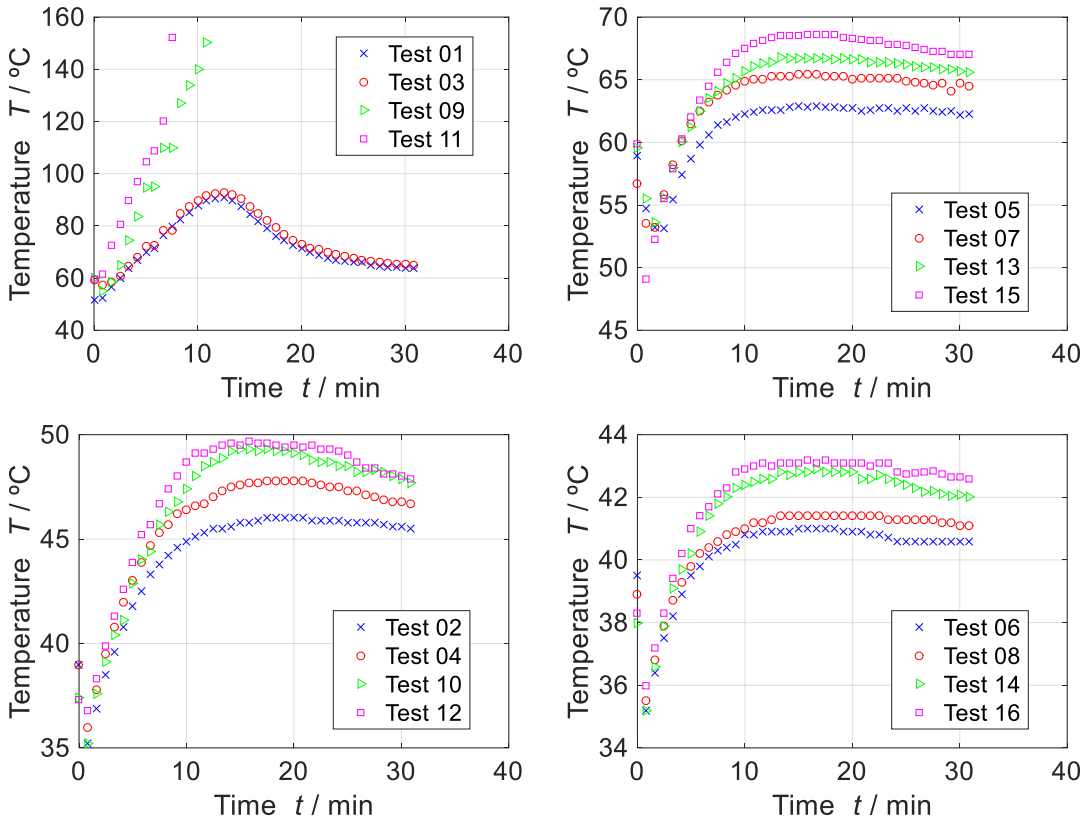

Figure 4. Experimental profiles of temperature T for Tests 01-16, as a function of the time t.

Table 2. Oxirane index (OI), iodine index (II), conversion (X), yield (Y) and selectivity (S) at the end of the reaction and maximum temperature value (T_{max}) for the experiments 01-16.

Test	OI / %	II / (g I_2/100 g)	X / %	Y / %	S	T_{max} / ºC
01	6.29	0.34	99.7	83.6	0.84	90.7
02	6.91	3.77	97.1	91.9	0.95	46.0
03	6.17	0.21	99.8	82.0	0.82	92.8
04	6.54	4.12	96.8	87.0	0.90	47.8
05	5.85	9.76	92.4	77.8	0.84	62.9

06	6.10	4.71	96.3	81.1	0.84	41.0
07	5.56	10.50	91.9	73.9	0.80	65.4
08	6.34	4.51	96.5	84.3	0.87	41.4
09	-	-	-	-	-	150.2
10	6.23	3.98	96.9	82.8	0.85	49.3
11	-	-	-	-	-	152.3
12	6.02	4.20	96.7	80.0	0.83	49.7
13	5.30	10.31	92.0	70.5	0.77	66.8
14	5.23	4.84	96.2	69.5	0.72	42.9
15	5.23	11.34	91.2	69.5	0.76	68.6
16	5.13	4.72	96.3	68.2	0.71	43.2

As seen in Figure 4, the conditions proposed in tests 09 and 11 led to a thermally unstable reaction system, i.e., the system underwent a thermal runaway accident. Despite the immersion of the reaction system in a controlled thermostatic bath, the heat transfer was not sufficient to remove the energy generated to avoid runaway. The temperature exceeded 90 ºC and reached a maximum value above 150 ºC, indicating that degradation of the hydrogen peroxide had occurred. Also, the reaction media was ejected from the reactor with great pressure. Therefore, the titration methods to measure the oxirane and iodine indexes were not performed for these tests.

Although the temperature for tests 01 and 03 exceeded 90 ºC, the reaction system seemed to remain under control (without runaway) and, after reaching a peak, the temperature dropped towards the temperature of the thermostatic bath. This suggests that the degradation reaction of hydrogen peroxide may not have occurred too vigorously under these conditions.

Comparing the temperature profiles for similar tests, apart from the stirring speed (i.e., tests 01 vs. 09, 02 vs. 10, 03 vs. 11, 04 vs. 12, 05 vs. 13, 06 vs. 14, 07 vs. 15 and 08 vs. 16), the higher the stirring speed, the lower the overshoot associated with the temperature profile. It is expected that the increase in the stirring speed would benefit both mass and heat transfer. These effects, in thermal terms, present opposite trends: the increase in heat transfer means that more energy can be removed from the system; conversely, the increase in mass transfer tends to intensify the exothermic reactions, i.e., enhancing the heat generated in the system. Nevertheless, the results indicated that the increase in the stirring speed tends to increase the heat transfer more significantly than the heat generated by the exothermic reactions. Therefore, within the range from 500 to 1000 rpm, higher stirring speeds tend to provide a more controlled environment for the reaction system. Additionally, at 1000 rpm, the tests resulted in similar double bond conversions, but considerably higher oxirane yield and selectivity than the ones at 500 rpm with similar conditions. This suggests that higher temperatures caused by lower stirring speeds (reduced heat transfer) tend to promote significantly faster kinetics of the ring-opening reactions.

The increase in the formic acid weight provoked a faster rise in the reaction system temperature, caused by the intensification of the reactions associated with higher availability of the limiting reactant. This condition, associated with a lower stirring speed, may be the most plausible explanation for the fast increase in the system temperature that caused the runaway in tests 09 and 11.

The use of higher amounts of formic acid also led to higher values for the double bonds conversion, oxirane yield and selectivity. This observation is physically coherent because the increase in the formic acid amount increases the availability of performic acid, hence intensifying the reaction. Nevertheless, the observed effect of this variable is opposite to the

trend observed by Campanella et al. [46], where an increase of the formic acid/double bond ratio did lead to higher double bond conversion, but with a decrease in the selectivity. A possible explanation for this discrepancy might be the difference in the reaction times – the present study performed the reaction during 4 h, while Campanella et al. studied the reaction system during 9-11.5 h. This increase in the reaction time also contributes to an intensification of the ring opening reactions, which are favored by lower pH (higher proton concentration derived from formic acid).

The effect of the hydrogen peroxide weight seemed to be the opposite with respect to the temperature profile, compared to the formic acid weight: lower amounts of hydrogen peroxide led to a slight increase in the overshoot of the reaction system temperature profile. Two thermal effects may be associated with the addition of the hydrogen peroxide solution: (1) a cooling effect on the reaction system, since the feed temperature of the hydrogen peroxide solution is lower than the reaction system temperature; (2) a decrease in the heat transfer, associated with an increase in the apparent viscosity due to the cooling effect, which would lead to an increase in the temperature of the system. Although these two possibilities lead to opposite trends concerning the temperature profiles, the experimental observations suggest that the effect (1) prevails over the effect (2). This is possibly the most plausible explanation, since this variable did not affect the *OI*, *II*, *X*, *Y* and *S* results in a systematic way. Therefore, it can be expected that the role of hydrogen peroxide in the ESO ring-opening reactions might not be significant, compared to formic acid, for example.

The main difference observed between the even tests, with a bath temperature of 40 ºC, and the odd tests, with a bath temperature of 60 ºC, was the smaller overshoot, comparing tests with similar conditions. This was due to the slower reaction rates, with the consequent reduction of

heat generation. Nonetheless, some of the even tests resulted in higher values of *OI* and lower values of *II* than the corresponding odd tests, as exemplified by a comparison between tests 05 and 06. Moreover, it is possible that the milder conditions of temperature, besides providing a safer operation, slow down the rate of the degradation reactions more than the main reactions, as evidenced by the fact that tests 02 and 04 resulted in the highest values of oxirane yield and selectivity. In particular, test 02 resulted in higher yield and selectivity values than test 04 due to the effect of formic acid.

The temperature profiles for tests 17-22 determined in our previous study [44] were employed for validation of the kinetic model. Test 17 also included profiles for *II* and *OI* with time, as shown in Figure 5. As can be observed from Figure 5a, the *II* values decrease asymptotically to a near null value (0.08 g/100 g I_2), after 4 h of reaction, which suggests reaction of almost all the double bonds of the soybean oil, with minimal interference of the undesired reaction of degradation of performic acid. Figure 5b presents the increase of *OI* to 6.72% with a peak value of 7.09% after 2 and 3 h of reaction, respectively, followed by a slight decrease to 7.05% at 4 h. From these profiles, one can conclude that it is possible to reach the industrial target of 6.5% after less than 2 h of reaction. Nevertheless, depending on the required target for *II*, which varies for each application, the reaction time could increase. These profiles also suggest that the undesired ring-opening reactions are relevant under the conditions of Test 17, especially between 3 and 4 h, because the theoretical (maximum) value of *OI* is 7.52%.

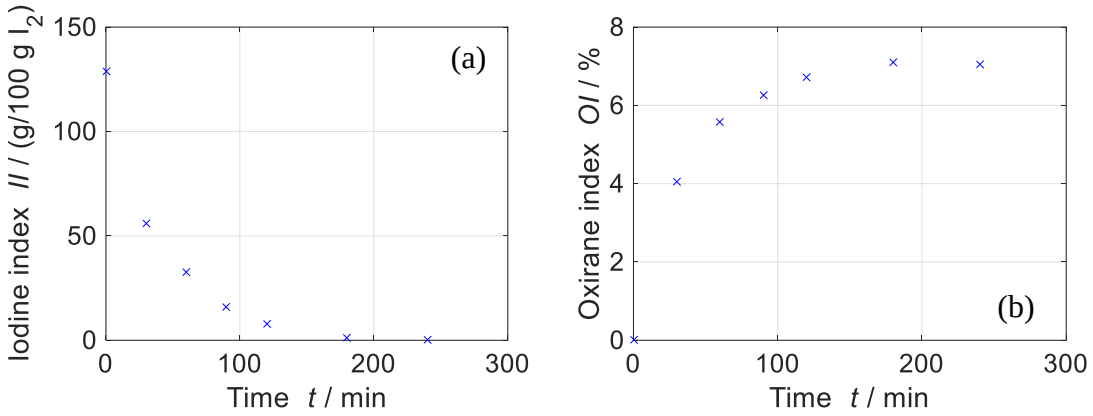

Figure 5. Experimental profiles for Test 17 as a function of time *t*: (a) iodine index, *II*; (b) oxirane index, *OI*.

Figure 6 presents the experimental profiles for the apparent kinematic viscosity of the reaction system for Tests 23-25. As can be observed, this property varies significantly with the reaction time, indicating that it is highly influenced by the conversion of the soybean oil double bonds. This is consistent with the correlation presented by Esteban et al. [45] that leads to a value of kinematic viscosity of 33.8×10^{-6} $m^2\cdot s^{-1}$ for soybean oil at 38 ºC, while our measurement of the kinematic viscosity of ESO at the same temperature is 210×10^{-6} $m^2\cdot s^{-1}$ (Figure 3). This apparent viscosity is also influenced by the stirring speed: higher stirring speeds tend to decrease the droplet size of the dispersed phase, which, in general, seems to increase the apparent viscosity of the present system.

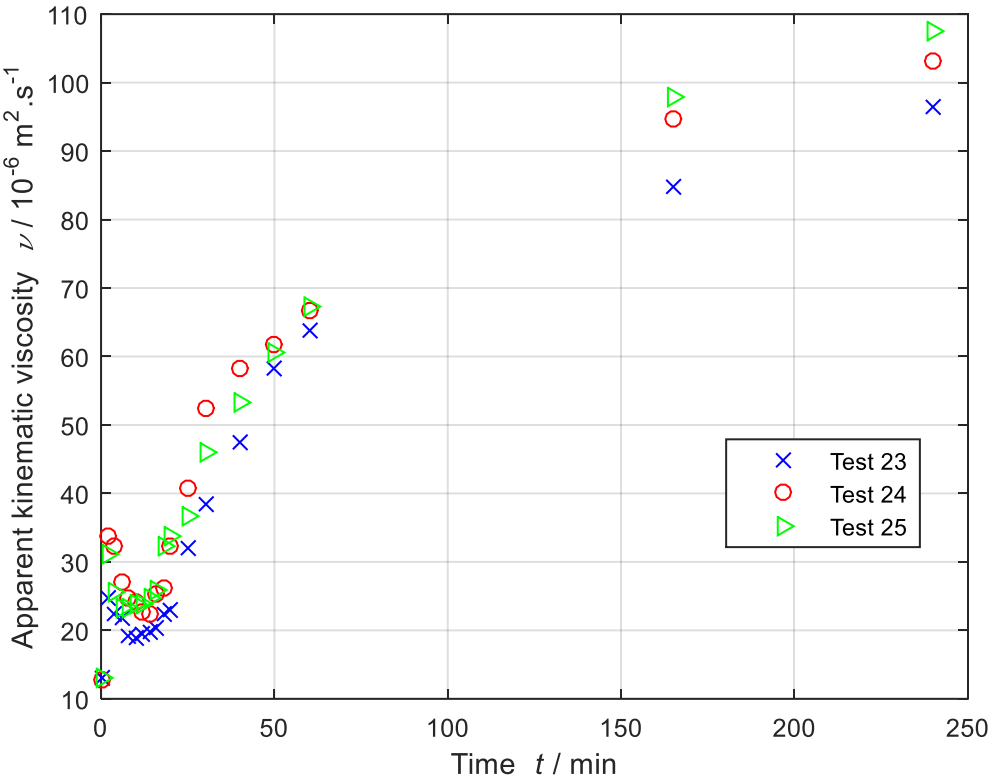

Figure 6. Experimental profiles of apparent kinematic viscosity v for Tests 23-25, as a function of time t.

3.2. Kinetic modeling

The kinetic modeling for the present reaction system took into account a fed-batch model during the feed interval of the hydrogen peroxide solution (t_{HPS}). After this period, a batch reactor model was assumed. Generically, for a component i in the phase j of the reaction system, the molar balance leads to Eq. (5), considering that the stirring is able to provide a homogeneous system.

$$\frac{dc_i^j}{dt} = \frac{fF_i^j + r_i^j V^j \pm J_i^j V^j}{V^j} - \frac{c_i^j}{V^j}\frac{dV^j}{dt} \tag{5}$$

where c is the molar concentration, t is the time, F is the molar flow rate in the feed, r is the kinetic rate, V is the volume, J is the mass transfer molar rate per unit of volume and the j superscript denotes either the aqueous phase (aq) or the organic phase (org). Here, the mass transfer term was considered to be negative for the aqueous phase and positive for the organic phase.

Considering that the whole feed of the system was only directed to the aqueous phase, the term related to the rate of change in the volume, present in Eq. (5), was applied solely for this phase, through Eq. (6).

$$\frac{dV^{aq}}{dt} = f\left(\frac{F_{HP}^{aq} M_{HP} + F_{W}^{aq} M_{W}}{\rho_{HPS}}\right) \tag{6}$$

in which M is the molar mass, ρ is the density and the subscripts HP, W and HPS denote, respectively, the hydrogen peroxide, the water and the hydrogen peroxide solution. Additionally, f is a binary factor, defined by Eq. (7).

$$f = \begin{cases} 1, & \text{if } t \leq t_{HPS} \\ 0, & \text{if } t > t_{HPS} \end{cases} \tag{7}$$

The molar flow was considered to be constant for both hydrogen peroxide and water, with values calculated for each test according to Eqs. (8) and (9), in which *w* represents the mass fraction.

$$F_{\mathrm{HP}}^{\mathrm{aq}} = \frac{w_{\mathrm{HP}} m_{\mathrm{HPS}}}{M_{\mathrm{HP}} t_{\mathrm{HPS}}} \tag{8}$$

$$F_{\mathrm{W}}^{\mathrm{aq}} = \frac{(1 - w_{\mathrm{HP}}) m_{\mathrm{HPS}}}{M_{\mathrm{W}} t_{\mathrm{HPS}}} \tag{9}$$

The kinetic law that describes the performic acid generation is given by Eq.(10), with *k* as the kinetic constant and *K* as the equilibrium constant. The subscripts FA, PFA and H^+ are related, respectively, to formic acid, performic acid, and protons [47].

$$r_1^{\mathrm{aq}} = k_1^{\mathrm{aq}} c_{\mathrm{H^+}}^{\mathrm{aq}} \left(c_{\mathrm{HP}}^{\mathrm{aq}} c_{\mathrm{FA}}^{\mathrm{aq}} - c_{\mathrm{PFA}}^{\mathrm{aq}} c_{\mathrm{W}}^{\mathrm{aq}} / K_1^{\mathrm{aq}} \right) \tag{10}$$

The Prileschajew reaction presents the kinetic law given in Eq. (11), in which the subscript DB refers to the double bonds of the soybean oil [47].

$$r_1^{\mathrm{org}} = k_1^{\mathrm{org}} c_{\mathrm{DB}}^{\mathrm{org}} c_{\mathrm{PFA}}^{\mathrm{org}} \tag{11}$$

For the degradation of performic acid, the literature proposes a first-order kinetic law [18], as described in Eq. (12).

$$r_2^{aq} = k_2^{aq} c_{PFA}^{aq} \quad (12)$$

The ring opening reactions of the ESO oxirane ring tend to occur in the interphase of the binary system, by a nucleophilic attack catalyzed by protons from formic acid. Here, the effect of the volumetric interfacial area (a_V) was also included. The kinetic laws for these reactions were described in Eqs. (13) to (16), with EG as the subscript for the epoxy group of the ESO.

$$r_2^{org} = k_2^{org} a_V c_{EG}^{org} c_{H^+}^{aq} c_{FA}^{aq} \quad (13)$$

$$r_3^{org} = k_3^{org} a_V c_{EG}^{org} c_{H^+}^{aq} c_{PFA}^{aq} \quad (14)$$

$$r_4^{org} = k_4^{org} a_V c_{EG}^{org} c_{H^+}^{aq} c_{W}^{aq} \quad (15)$$

$$r_5^{org} = k_4^{org} a_V c_{EG}^{org} c_{H^+}^{aq} c_{HP}^{aq} \quad (16)$$

Although there are substances from both phases involved in the ring opening reactions, the kinetic constants were determined based on the volume of the disperse phase of the system.

The temperature dependence of the kinetic constant q in the phase j was described by the Arrhenius equation, using the reference value $k_{q,r}^{j}$ at a reference temperature T_r, as stated in Eq. (17).

$$k_q^j = k_{q,r}^j \exp\left[\left(E_q^j/R\right)\left(1/T_r - 1/T\right)\right] \tag{17}$$

in which E is the activation energy, R is the universal gas constant and T is the absolute temperature.

Similarly, the equilibrium constant for the reaction of generation of performic acid was described as a function of the temperature through the van't Hoff's equation, Eq. (18), using the corresponding value of the enthalpy of reaction (ΔH).

$$K_1^{aq} = K_{1,r}^{aq} \exp\left[\left(\Delta H_1^{aq}/R\right)\left(1/T_r - 1/T\right)\right] \tag{18}$$

After defining the kinetic laws for all the reactions considered in the present model, Eq. (5) can be described for each component, considering that the mass transfer applies only for formic and performic acids, leading to Eqs. (19) to (26):

$$\frac{dc_{FA}^{aq}}{dt} = -r_1^{aq} - r_2^{org} - J_{FA}^{aq} - \frac{c_{FA}^{aq}}{V^{aq}}\frac{dV^{aq}}{dt} \tag{19}$$

$$\frac{dc_{HP}^{aq}}{dt} = = -r_1^{aq} - r_5^{org} + \frac{fF_{HP}^{aq}}{V^{aq}} - \frac{c_{HP}^{aq}}{V^{aq}}\frac{dV^{aq}}{dt} \tag{20}$$

$$\frac{dc_{PFA}^{aq}}{dt} = r_1^{aq} - r_3^{org} - J_{PFA}^{aq} - \frac{c_{PFA}^{aq}}{V^{aq}}\frac{dV^{aq}}{dt} \tag{21}$$

$$\frac{\mathrm{d}c_{\mathrm{W}}^{\mathrm{aq}}}{\mathrm{d}t} = r_1^{\mathrm{aq}} - r_4^{\mathrm{org}} + \frac{fF_{\mathrm{W}}^{\mathrm{aq}}}{V^{\mathrm{aq}}} - \frac{c_{\mathrm{W}}^{\mathrm{aq}}}{V^{\mathrm{aq}}}\frac{\mathrm{d}V^{\mathrm{aq}}}{\mathrm{d}t} \tag{22}$$

$$\frac{\mathrm{d}c_{\mathrm{PFA}}^{\mathrm{org}}}{\mathrm{d}t} = -r_1^{\mathrm{org}} + J_{\mathrm{PFA}}^{\mathrm{org}} \tag{23}$$

$$\frac{\mathrm{d}c_{\mathrm{DB}}^{\mathrm{org}}}{\mathrm{d}t} = -r_1^{\mathrm{org}} \tag{24}$$

$$\frac{\mathrm{d}c_{\mathrm{FA}}^{\mathrm{org}}}{\mathrm{d}t} = r_1^{\mathrm{org}} + J_{\mathrm{FA}}^{\mathrm{org}} \tag{25}$$

$$\frac{\mathrm{d}c_{\mathrm{EG}}^{\mathrm{org}}}{\mathrm{d}t} = r_1^{\mathrm{org}} - \left(r_2^{\mathrm{org}} + r_3^{\mathrm{org}} + r_4^{\mathrm{org}} + r_5^{\mathrm{org}}\right)\frac{V^{\mathrm{aq}}}{V^{\mathrm{org}}} \tag{26}$$

The proton concentration was estimated through the equilibrium constant (K_a) associated with the ionization reaction of the formic acid, which can be related to the pK_a of formic acid, according to Eq. (27).

$$c_{\mathrm{H^+}}^{\mathrm{aq}} = \sqrt{c_{\mathrm{FA}}^{\mathrm{aq}} K_a} = \sqrt{c_{\mathrm{FA}}^{\mathrm{aq}} 10^{-\mathrm{p}K_a}} \tag{27}$$

Eq. (28) describes the temperature dependence of the formic acid pK_a [48].

$$\mathrm{p}K_a = -57.528 + 2773.9/T\,[\mathrm{K}] + 9.1232 \ln T\,[\mathrm{K}] \tag{28}$$

The mass transfer effects were described based on Whitman's theory [49], establishing that there is a film with a given thickness in the interphase between the aqueous and organic phases, making the mass transfer occur exclusively by diffusion. Then, the J values can be calculated with Eqns. (29) and (30):

$$J_i^{aq} = \beta_i^{aq} a_V \left(c_i^{aq} - c_i^{org,eq} H_i \right) \tag{29}$$

$$J_i^{org} = \beta_i^{org} a_V \left(c_i^{org,eq} - c_i^{org} \right) \tag{30}$$

in which β is the mass transfer coefficient, H is the partition coefficient between phases and the superscript eq denotes the equilibrium concentration.

According to Santacesaria et al. [26], the β value for the organic phase can be determined after the corresponding value for the aqueous phase through Eq. (31). In addition, since formic and performic acids present similar structures, the same values of β were considered for these substances in each phase.

$$\beta^{org} = \beta^{aq} V^{aq} / V^{org} \tag{31}$$

The hypothesis of no accumulation of the components at the interphase leads to Eq. (32) in order to determine the equilibrium concentration for formic and performic acids at the organic phase.

$$c_i^{\mathrm{org,eq}} = \frac{\beta^{\mathrm{aq}} c_i^{\mathrm{aq}} V^{\mathrm{aq}} + \beta^{\mathrm{org}} c_i^{\mathrm{org}} V^{\mathrm{org}}}{\beta^{\mathrm{aq}} H_i V^{\mathrm{aq}} + \beta^{\mathrm{org}} V^{\mathrm{org}}} = \frac{c_i^{\mathrm{aq}} + c_i^{\mathrm{org}}}{H_i + 1} \tag{32}$$

Eqs. (33) and (34) describe the temperature dependence of the partition coefficients [26].

$$H_{\mathrm{FA}} = c_{\mathrm{FA}}^{\mathrm{aq,eq}} / c_{\mathrm{FA}}^{\mathrm{org,eq}} = \left[9{\cdot}10^{-7}(T\,[\mathrm{K}])^2 - 5.42{\cdot}10^{-4}\,T\,[\mathrm{K}] + 0.0854\right]^{-1} \tag{33}$$

$$H_{\mathrm{PFA}} = c_{\mathrm{PFA}}^{\mathrm{aq,eq}} / c_{\mathrm{PFA}}^{\mathrm{org,eq}} = \left[4{\cdot}10^{-6}(T\,[\mathrm{K}])^2 - 2.23{\cdot}10^{-3}\,T\,[\mathrm{K}] + 0.3496\right]^{-1} \tag{34}$$

The volumetric interfacial area was calculated with Eq. (35) based on the assumption that the dispersed phase of the system consists on drops with spherical morphology, with a Sauter mean diameter D_{32}.

$$a_{\mathrm{V}} = 6/D_{32} \tag{35}$$

The value of D_{32} was estimated iteratively with Eq. (36) [50].

$$(D_{32}/D_{\mathrm{I}}) = \alpha_1(1 + \alpha_2\phi)[1 + \alpha_3 VN(D_{32}/D_{\mathrm{I}})^{\alpha_4}]We^{\alpha_5} \tag{36}$$

in which ϕ is the holdup, VN is the viscosity number, We is the Weber number, D_I is the impeller diameter and α_1, α_2, α_3, α_4 and α_5 are parameters that were already estimated for the present system by Wu et al. [29].

The holdup was determined as the volumetric fraction of the dispersed phase, Eq. (37). Here the dispersed phase was considered to be the aqueous phase, similarly to Wu et al. [29].

$$\phi = V^{aq}/(V^{aq} + V^{org}) \tag{37}$$

The viscosity number and the Weber number were calculated from Eqs. (38) and (39), in which μ_d is the dynamic viscosity of the dispersed phase, ρ_c is the density of the continuous phase, N is the stirring speed and σ is the interfacial tension.

$$VN = \mu_d N D_I/\sigma \tag{38}$$

$$We = \rho_c N^2 D_I^3/\sigma \tag{39}$$

The energy balance led to Eq. (40), in which C_p is the heat capacity on a mass basis, U is the global heat transfer coefficient, A is the heat transfer area, T_b is the bath temperature and T_{HPS} is the feed temperature of the hydrogen peroxide solution.

$$\frac{dT}{dt} = \frac{\sum_j \left\{\left[\sum_q \left(-\Delta H_q^j\right) r_q^j\right] V^j\right\} - UA(T - T_b)}{\sum_j \left(\rho^j V^j C_p^j\right)} - \frac{f\left(F_{HP}^{aq} M_{HP} + F_W^{aq} M_W\right) C_{p,HPS}(T - T_{HPS})}{\sum_j \left(\rho^j V^j C_p^j\right)} \quad (40)$$

The global heat transfer coefficient was described with Eq. (41) as a function of the apparent kinematic viscosity of the reaction system (v) and the stirring speed. The parameters of this equation, p_1 and p_2, are related to a combination of several values, such as the impeller and reactor diameters and the density, heat capacity and thermal conductivity of the reaction system, negligible effects when compared to the kinematic viscosity and stirring speed, as described in Appendix A.

$$U = 1/\left(p_1 v^{1/3} N^{-2/3} + p_2\right) \quad (41)$$

The density and heat capacity of the aqueous phase were described in Eqs. (42) and (43) as a function of the corresponding values for the hydrogen peroxide and formic acid solutions.

$$\rho^{aq} = \left(m_{HPS} + m_{FAS}\right)/\left(m_{HPS}/\rho_{HPS} + m_{FAS}/\rho_{FAS}\right) \quad (42)$$

$$C_p^{aq} = \left(m_{HPS} C_{p,HPS} + m_{FAS} C_{p,FAS}\right)/\left(m_{HPS} + m_{FAS}\right) \quad (43)$$

The values of ρ_{HPS}, ρ_{FAS}, $C_{p,HPS}$ and $C_{p,FAS}$ were estimated and described as a function of the temperature, respectively in Eqs. (44) to (47), based on literature data [51–53].

$$\rho_{\mathrm{HPS}}\left[\mathrm{g{\cdot}L^{-1}}\right] = 1507.6 - 0.9117T\,[\mathrm{K}] \tag{44}$$

$$\rho_{\mathrm{FAS}}\left[\mathrm{g{\cdot}L^{-1}}\right] = 1507.8 - 1.1169T\,[\mathrm{K}] \tag{45}$$

$$C_{p,\mathrm{HPS}}\left[\mathrm{J{\cdot}g^{-1}{\cdot}K^{-1}}\right] = 3.25 \tag{46}$$

$$C_{p,\mathrm{FAS}}\left[\mathrm{J{\cdot}g^{-1}{\cdot}K^{-1}}\right] = 2.088 + 1.2682{\cdot}10^{-3}\,T\,[\mathrm{K}] \tag{47}$$

The dynamic viscosity of the aqueous phase, required in Eq. (38), was considered to be equal to the value of pure water, which was estimated as a function of the temperature in Eq. (48) [29].

$$\mu^{\mathrm{aq}}[\mathrm{Pa{\cdot}s}] = \mu_{\mathrm{d}} = 1.8588{\cdot}10^{-4}\exp[54.640/(T\,[\mathrm{K}] - 273.15)] \tag{48}$$

The density and heat capacity of the organic phase were approximated as the values of pure soybean oil, defined by Eqs.(49) and (50), respectively [51].

$$\rho^{\mathrm{org}}\left[\mathrm{g{\cdot}L^{-1}}\right] = \rho_{\mathrm{c}} = 1112.9 - 0.657T\,[\mathrm{K}] \tag{49}$$

$$C_p^{\mathrm{org}}\left[\mathrm{J{\cdot}g^{-1}{\cdot}K^{-1}}\right] = 1.0201 + 2.9412{\cdot}10^{-3}\,T\,[\mathrm{K}] \tag{50}$$

Lastly, the apparent kinematic viscosity of the reaction system, required in Eq. (41), was expressed as a variation of the Andrade equation [54], including the effects of the stirring speed and the double bond conversion, according to Eq. (51), with p_3, p_4, p_5 and p_6 as parameters.

$$\nu = \left[p_3 + \left(p_4 + p_5 N\right)X\right]\exp\left[p_6/(T - 273.15)\right] \tag{51}$$

The constant values used in the kinetic model collected from the literature or dependent on the conditions of the experiments are summarized in Table 3.

Table 3. Parameters collected from the literature and experimental conditions.

Parameter	Reaction	Value	Unit	Reference
$K_{1,r}^{aq}$ at T_r = 70 ºC	PFA synthesis	0.95		[55]
ΔH_1^{aq}	PFA synthesis	-10781	J·mol^{-1}	Estimated from [55]
ΔH_2^{aq}	PFA degradation	-235478	J·mol^{-1}	Estimated from [37,56]
ΔH_1^{org}	Epoxidation	-174723	J·mol^{-1}	Estimated from [37]
ΔH_2^{org}	ESO degradation by formic acid	37710	J·mol^{-1}	Estimated from [37]
ΔH_3^{org}	ESO degradation by performic acid	37710	J·mol^{-1}	Estimated from [37]
ΔH_4^{org}	ESO degradation by water	12570	J·mol^{-1}	Estimated from [37]
ΔH_5^{org}	ESO degradation by hydrogen peroxide	12570	J·mol^{-1}	Estimated from [37]
M_{I_2}		253.8	g·mol^{-1}	
M_O		16.0	g·mol^{-1}	

M_{HP}	34.0	g·mol^{-1}	
M_W	18.0	g·mol^{-1}	
w_{HP}	0.60		
t_{HPS}	30-120	s	
T_{HPS}	298.15	K	
A	0.0201	m^2	
D_I	0.06	m	
α_1	0.1422		[29]
α_2	1.1467		[29]
α_3	22658		[29]
α_4	1.7669		[29]
α_5	-0.5731		[29]
σ	0.02	N·m^{-1}	[29]

Besides the values collected from the literature, the model presents 21 parameters, which were determined by the fit of the model to experimental data: $k_{1,r}^{aq}$, E_1^{aq}, $k_{2,r}^{aq}$, E_2^{aq},$k_{1,r}^{org}$, E_1^{org},$k_{2,r}^{org}$, E_2^{org},$k_{3,r}^{org}$, E_3^{org},$k_{4,r}^{org}$, E_4^{org},$k_{5,r}^{org}$, E_5^{org},β^{aq}, p_1, p_2, p_3, p_4, p_5 and p_6. The strategy for the estimation of these parameters is schematically described on Figure 7, coupled with the optimization of the objective functions (*OF*) expressed in Eqs. (52) to (54), where n_{exp} is the number of experimental data for each variable and the subscripts "exp" and "mod" refer to the experimental measurement and the value predicted by the model, respectively. The parameters were carefully grouped based on the relative impact on each objective function. Nevertheless, it can be emphasized that all of the parameters directly or indirectly impact all of the *OF*. The optimization procedure was assisted by MATLAB (version R2105a), using the Levenberg-Marquardt algorithm.

$$OF_1 = \min_{k_{1,f}^{aq}, E_1^{aq}, k_{1,f}^{org}, E_1^{org}, \beta^{aq}, p_1 p_2} \sum_{i=1}^{n_{exp,T}} \left(T_{i,exp} - T_{i,mod}\right)^2 \tag{52}$$

$$OF_2 = \min_{p_3 p_4 p_5 p_6} \sum_{i=1}^{n_{exp,v}} \left(v_{i,exp} - v_{i,mod}\right)^2 \tag{53}$$

$$OF_3 = \min_{\substack{k_{2,f}^{aq}, E_2^{aq}, k_{2,f}^{org}, E_2^{org}, k_{3,f}^{org}, \\ E_3^{org}, k_{4,f}^{org}, E_4^{org}, k_{5,f}^{org}, E_5^{org}}} \sum_{i=1}^{n_{exp,II}} \left(\frac{II_{i,exp} - II_{i,mod}}{II_0}\right)^2 + \sum_{i=1}^{n_{exp,OI}} \left(\frac{OI_{i,exp} - OI_{i,mod}}{OI_t}\right)^2 \tag{54}$$

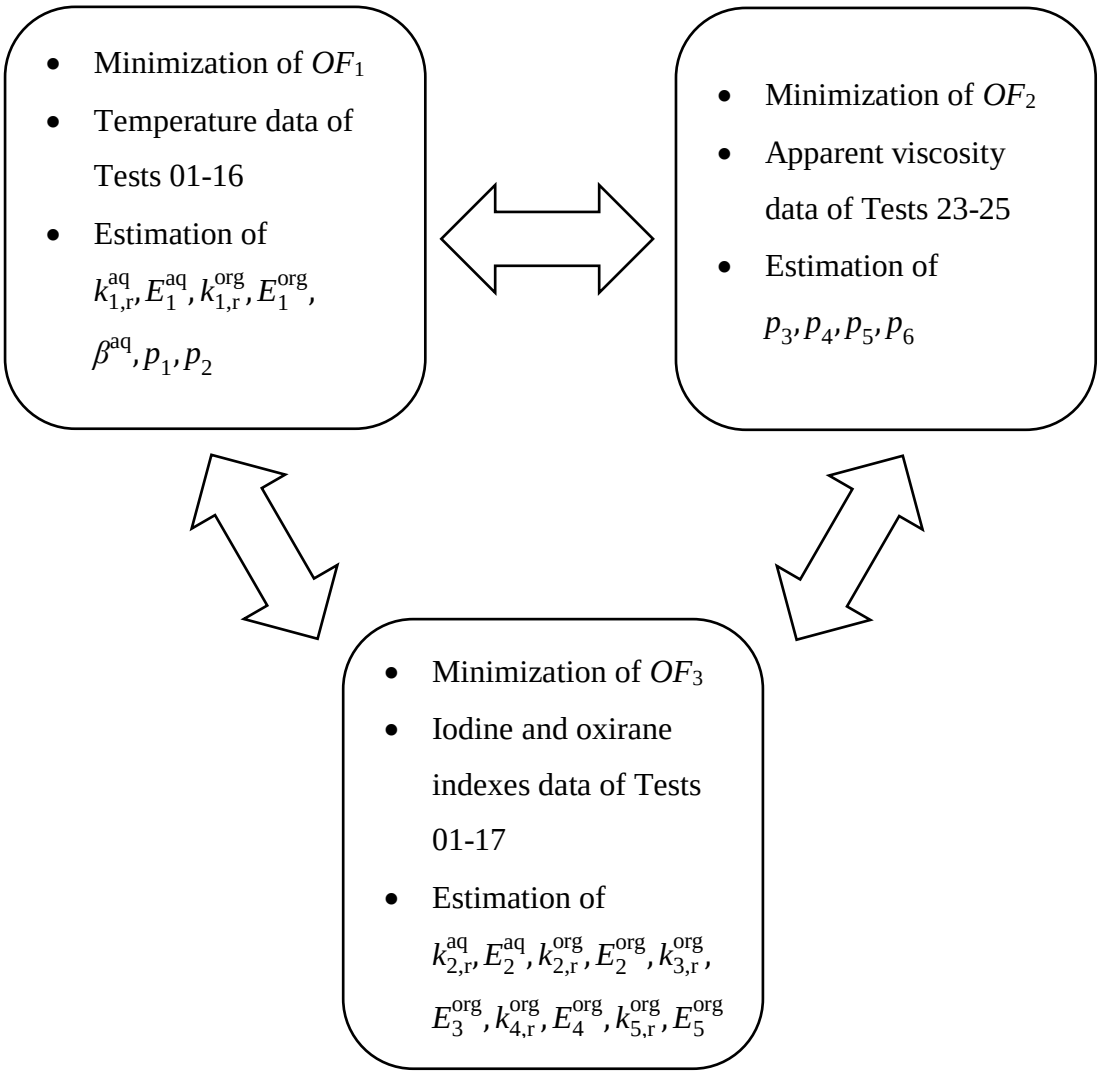

Figure 7. Strategy for the estimation of the parameters of the kinetic model.

The optimized values of the 21 parameters are collected in Table 4, together with the respective 95% confidence interval. The comparison of these values with the literature is quite difficult to perform, since a wide range of values and different experimental conditions were found. For the reaction to produce performic acid, for example, Zheng et al. [31] estimated a kinetic constant of 0.15 $L \cdot mol^{-1} \cdot s^{-1}$ at 66.85 ºC, different from the value reported here and in other studies from the literature. Nevertheless, the value of 5.49×10^{-3} $L^2 \cdot mol^{-2} \cdot s^{-1}$ at 70 ºC presented

here agrees with the values of 1.69×10^{-3} $L^2\cdot mol^{-2}\cdot s^{-1}$ and 1.09×10^{-2} $L^2\cdot mol^{-2}\cdot s^{-1}$ estimated at 70 ºC from the studies of Wu et al. [27] and Santacesaria et al. [26], respectively. The value of 5.09×10^4 $J\cdot mol^{-1}$ for the activation energy of this reaction also agrees well with reported values of 47724 $J\cdot mol^{-1}$ [26], 46000 $J\cdot mol^{-1}$ [27], 44270 $J\cdot mol^{-1}$ [18] and 43524 $J\cdot mol^{-1}$ [29], although values of 11390 $J\cdot mol^{-1}$ [26] and 150000 $J\cdot mol^{-1}$ [31] were also reported. It is noteworthy that all these values were estimated based on the volume of the aqueous phase.

The literature values for the kinetic constant of the epoxidation reaction cover a wide range, with different orders of magnitude, from 2.80×10^{-5} $L\cdot mol^{-1}\cdot s^{-1}$ [28] to 2.23 $L\cdot mol^{-1}\cdot s^{-1}$ [26], both evaluated at the reference temperature of 70 ºC. Nevertheless, the value of 7.30×10^{-2} $L\cdot mol^{-1}\cdot s^{-1}$ determined here is the same order of magnitude as the values of 3.33×10^{-2} $L\cdot mol^{-1}\cdot s^{-1}$ [26], 1.02×10^{-2} $L\cdot mol^{-1}\cdot s^{-1}$ [18] and 4.04×10^{-2} $L\cdot mol^{-1}\cdot s^{-1}$ [29] estimated at 70 ºC. Moreover, the value of 3.80×10^4 $J\cdot mol^{-1}$ for the activation energy of the epoxidation reaction is in the literature range between 24890 $J\cdot mol^{-1}$ [28] and 104289 $J\cdot mol^{-1}$ [26], showing the best agreement with the values 41000 $J\cdot mol^{-1}$ [27] and 40285 $J\cdot mol^{-1}$ [18].

A wide range was also found in the literature for the kinetic constant for performic acid degradation at 70 ºC from 1.25×10^{-9} s^{-1} [18] to 5.67×10^{-2} s^{-1} [29]. The value of 2.00×10^{-4} s^{-1} reported here is inside this range and the same order of magnitude as 5.90×10^{-4} s^{-1} [27], evaluated at the same temperature. Nevertheless, the activation energy presented here (9.75×10^4 $J\cdot mol^{-1}$) disagrees with the literature range between 20000 $J\cdot mol^{-1}$ [31] and 77716 $J\cdot mol^{-1}$ [18]. Despite this, the authors believe that a higher value represents the physical behavior of this reaction, in which CO_2 may be generated more intensely at higher temperatures.

The kinetic equation for the ring opening reactions of the epoxy group can be described through different formulations, in which some authors considerer the protonation of the oxygen

atom of the epoxy group as the rate determining step in order to simplify the kinetic law, eliminating the effect of different nucleophiles [26–28,47]. Moreover, other studies that reported parameters of these kinetic laws did not include the effect of the interfacial area [18,29,31], complicating the comparison of the numerical values of these parameters. Nevertheless, it is notable here that there is a systematic decrease in the order of magnitude for the ring opening reactions: $k_{3,r}^{org} > k_{2,r}^{org} > k_{5,r}^{org} \approx k_{4,r}^{org}$, similar to the values determined by Zheng et al. [31] and Wu et al. [29].

This is also in agreement with the experimental studies of Campanella and Baltanás [19,20] and Cai et al. [22] using acetic acid, in which the ring opening reactions by nucleophilic attack of the acid and the peracid were more relevant than the reactions of water and hydrogen peroxide. Moreover, this also agrees with the experimental evidence in the present study that the amount of hydrogen peroxide did not significantly affect the oxirane yield and the selectivity.

In addition, it is also noteworthy to mention the results for the global heat transfer coefficient and for the volumetric interfacial area: the average value for U was 250.63 $W \cdot m^{-2} \cdot K^{-1}$, in the range between 219.06 and 282.57 $W \cdot m^{-2} \cdot K^{-1}$; for a_V, the average value was 34639 m^{-1}, with 17098 and 62611 m^{-1} as the respective minimum and maximum values. The aim of presenting these wide ranges is to highlight the importance of including correlations in the model to describe them as a function of the system conditions.

Table 4. Optimized parameters of the kinetic model coupled with the corresponding 95% confidence intervals.

Parameter	Reaction	Value	Unit
$k_{1,r}^{aq}$ at T_r = 70 ºC	PFA synthesis	(5.49 ± 0.10) ×10^{-3}	$L^2 \cdot mol^{-2} \cdot s^{-1}$

$k_{2,r}^{aq}$ at T_r = 70 ºC	PFA degradation	$(2.00 \pm 0.04)\times10^{-4}$	s^{-1}
$k_{1,r}^{org}$ at T_r = 70 ºC	Epoxidation	$(7.30 \pm 0.48)\times10^{-2}$	$L\cdot mol^{-1}\cdot s^{-1}$
$k_{2,r}^{org}$ at T_r = 70 ºC	ESO degradation by formic acid	$(3.43 \pm 0.04)\times10^{-8}$	$L^2\cdot m\cdot mol^{-2}\cdot s^{-1}$
$k_{3,r}^{org}$ at T_r = 70 ºC	ESO degradation by performic acid	$(2.90 \pm 0.03)\times10^{-7}$	$L^2\cdot m\cdot mol^{-2}\cdot s^{-1}$
$k_{4,r}^{org}$ at T_r = 70 ºC	ESO degradation by water	$(1.43 \pm 0.06)\times10^{-9}$	$L^2\cdot m\cdot mol^{-2}\cdot s^{-1}$
$k_{5,r}^{org}$ at T_r = 70 ºC	ESO degradation by hydrogen peroxide	$(4.78 \pm 0.01)\times10^{-9}$	$L^2\cdot m\cdot mol^{-2}\cdot s^{-1}$
E_1^{aq}	PFA synthesis	$(5.09 \pm 0.11)\times10^{4}$	$J\cdot mol^{-1}$
E_2^{aq}	PFA degradation	$(9.75 \pm 0.06)\times10^{4}$	$J\cdot mol^{-1}$
E_1^{org}	Epoxidation	$(3.80 \pm 0.39)\times10^{4}$	$J\cdot mol^{-1}$
E_2^{org}	ESO degradation by formic acid	$(4.75 \pm 0.04)\times10^{4}$	$J\cdot mol^{-1}$
E_3^{org}	ESO degradation by performic acid	$(9.54 \pm 0.04)\times10^{4}$	$J\cdot mol^{-1}$
E_4^{org}	ESO degradation by water	$(5.85 \pm 0.04)\times10^{4}$	$J\cdot mol^{-1}$
E_5^{org}	ESO degradation by hydrogen peroxide	$(2.87 \pm 0.05)\times10^{4}$	$J\cdot mol^{-1}$
β^{aq}		$(5.30 \pm 0.01)\times10^{-5}$	m·s-1
p_1		$(8.01 \pm 0.12)\times10^{-2}$	$s^{8/3}\cdot K\cdot m^{-2/3}\cdot kg^{-1}$
p_2		$(3.21 \pm 0.10)\times10^{-3}$	$s^{3}\cdot K\cdot kg^{-1}$
p_3		$(1.45 \pm 0.06)\times10^{-6}$	$m^2\cdot s^{-1}$
p_4		$(4.18 \pm 0.69)\times10^{-6}$	$m^2\cdot s^{-1}$
p_5		$(6.53 \pm 0.45)\times10^{-8}$	m^2
p_6		$(1.70 \pm 0.06)\times10^{2}$	K

Figure 8 displays the temperature profiles predicted by the model in comparison with the experimental values for Tests 01-16. Here, Tests 09 and 11 were not represented, due to the observed runaway of the system, which may have included other factors that were not considered in the development of the present kinetic modeling, such as hydrogen peroxide decomposition. Hence, apart from these two tests, it is notable that the model is able to represent the tendency of the experimental data for the temperature. This also encompasses the decrease of the temperature in the initial instants due to the hydrogen peroxide addition. The standard deviation associated with the fit of the model to the temperature data was determined as 1.43 ºC.

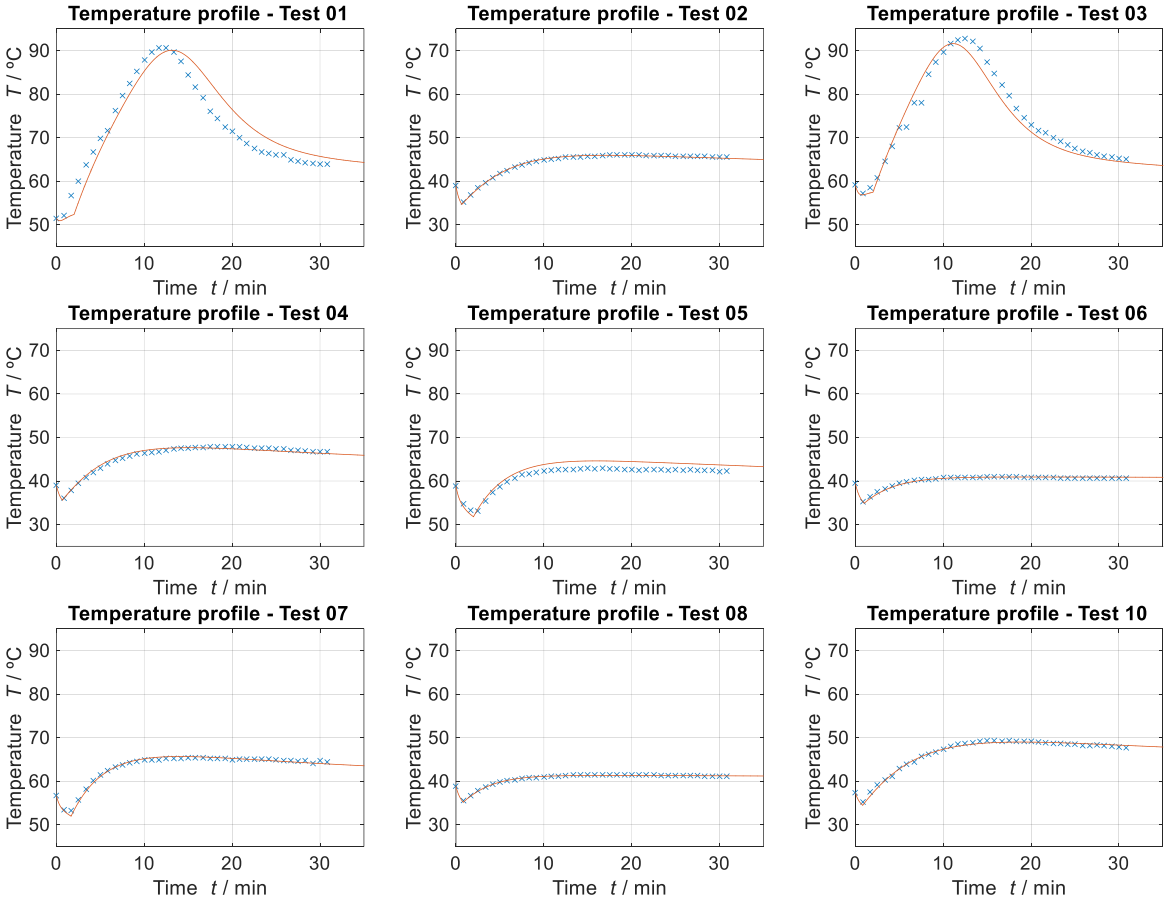

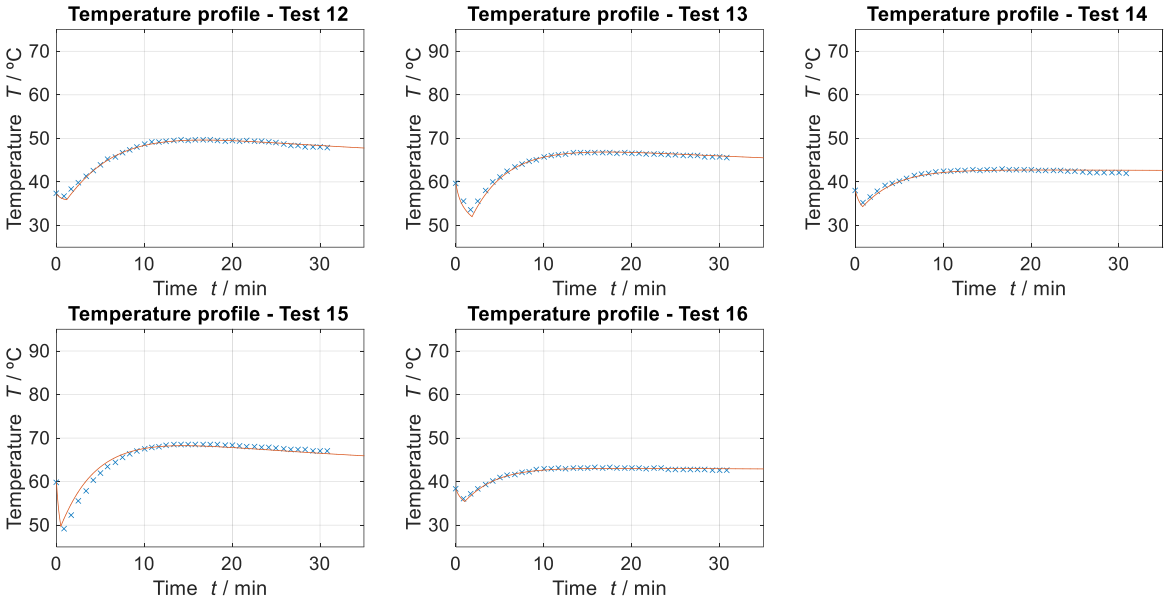

Figure 8. Profiles of temperature T for Tests 01-16, as a function of time t: (×), experimental values; (—), values predicted by the model.

The profiles for the kinematic viscosity are shown in Figure 9, comparing the experimental values of Tests 23-25 with the values predicted by the model. Similar to the temperature profiles, a good agreement between the experimental and the model values can be observed, validating the proposed equation (51). The standard deviation between the model prediction and the experimental data was 3.98×10^{-6} $m^2 \cdot s^{-1}$.

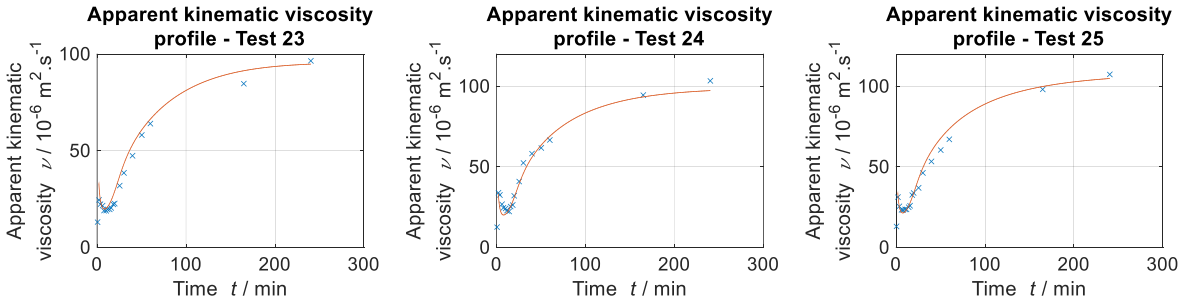

Figure 9. Profiles of apparent kinematic viscosity *v* for Tests 23-25, as a function of time *t*: (×), experimental values; (—), values predicted by the model.

The results of the kinetic modeling concerning the iodine index and oxirane index are presented in Figure 10 for Tests 01-16 (in which measurements were carried out only at the end of the batch) and Figure 11 for Test 17 (in which the measurements were carried out at time intervals during the entire batch).

The lack of a better fitting of the data in Figure 10 can be explained by the fact that these measurements were performed only at the end of the reaction (4 h), but without a sharp quench to interrupt the reaction. At the end of the batch, the agitation was stopped and the reactor taken out of the thermostatic bath and left to settle and cool down at ambient temperature for 24 h. Hence, it is quite probable that the reactions may have continued during the slow cooling down period after the end of the batch, thus impacting the quality of these experimental data.

In counterpoint, Figure 11 provides a very good fit of the *II* and *OI* profiles for the conditions of Test 17. Good agreement of the model with the experimental profiles can be observed for both properties in this run. In this test, small samples were withdrawn from the reactor at time intervals along the experiment and then quickly quenched to stop the reaction; therefore, the measurements of *II* and *OI* are certainly much more reliable in Test 17 than in the other experiments. Overall, considering the results from Tests 01-17, the standard deviations concerning the modeling of the experimental data of *II* and *OI* were, respectively, 6.69 g/100 g I_2 and 0.92%.

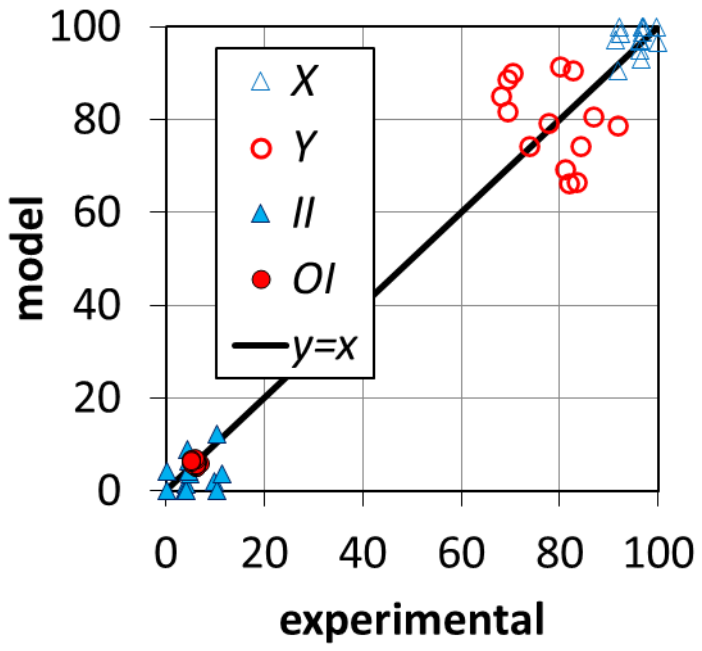

Figure 10. Comparison between the experimental data and values calculated by the model for the iodine index (*II*), oxirane index (*OI*), double bond conversion (*X*) and oxirane yield (*Y*) for Tests 01-16 (measurements made only at the final time of each run, after slow settling and cooling down of the reactor contents).

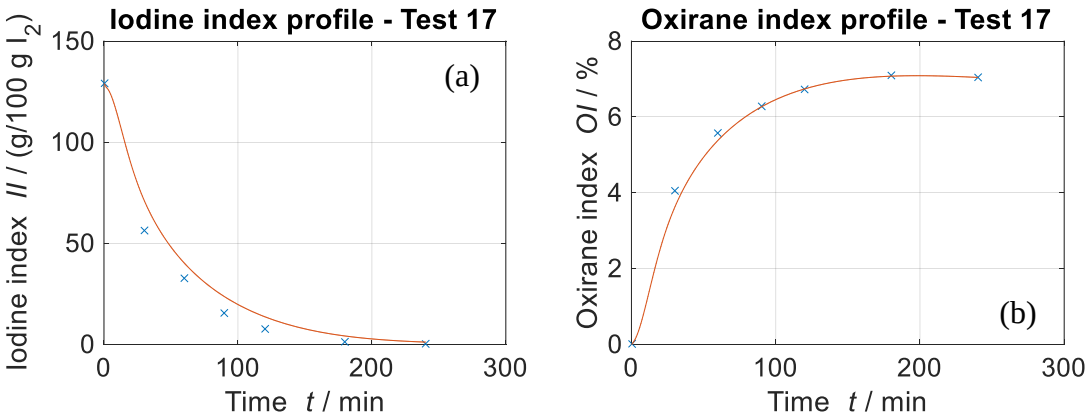

Figure 11. Profiles for Test 17 as a function of time *t*: (a) iodine index (*II*); (b) oxirane index (*OI*); (×), experimental values; (—), values predicted by the model.

Lastly, Figure 12 shows the temperature profiles for the conditions of Tests 17-23 with different numbers of peroxide additions. As mentioned before, these profiles were not applied for the estimation of the kinetic model parameters. These values were used for validation of the kinetic model after the determination of the parameters. Similarly to Figure 8, the agreement between the temperature profiles predicted from the model and the experimental data is noteworthy, concerning the overshoot tendency and the decrease in temperature due to the hydrogen peroxide additions. Here the standard deviation associated with this prediction was 1.2 ºC.

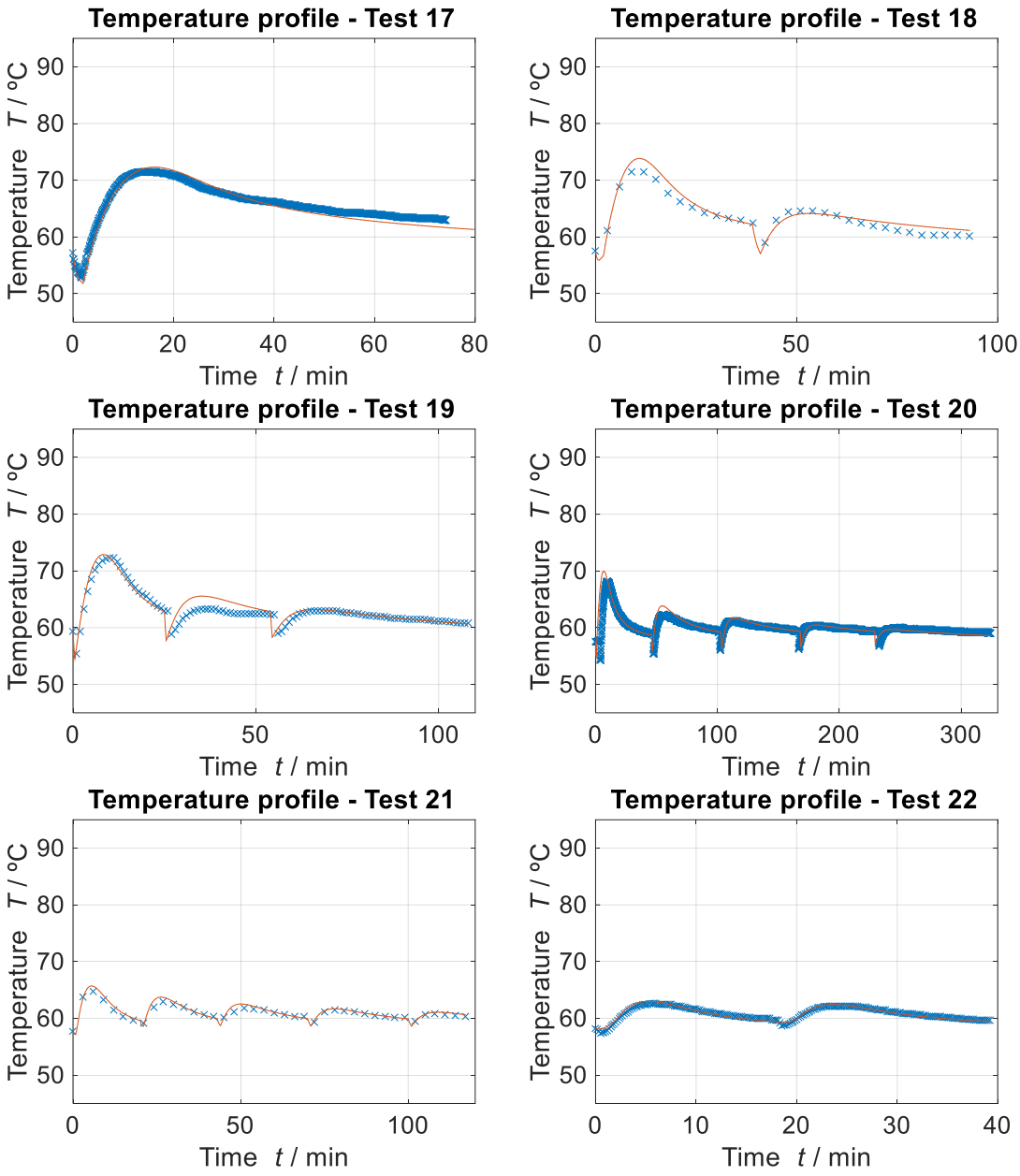

Figure 12. Profiles of temperature T for Tests 17-23 as a function of time t: (×), experimental values; (—), values predicted by the model.

4. Conclusion

The present study encompassed an experimental analysis of the reaction system for the epoxidation of soybean oil with a single addition of the reactants without the inclusion of other catalysts. The first experiments (Tests 01-16) were based on a 2^k factorial planning (k = 4) in order to verify the effects of the amounts of hydrogen peroxide solution, formic acid solution, temperature of the thermostatic bath and stirring speed. The main conclusions from these experiments were the achievement of lower temperature overshoots using lower bath temperatures and higher stirring speeds, especially with higher amounts of formic acid. After 4 h of reaction, followed by 24 h of decantation, Test 02, with milder conditions of bath temperature, presented the highest values of yield (91.9%) and selectivity (0.95). The experimental Test 17 followed the evolution of the oxirane index and the decrease of the iodine index with time, introducing reaction conditions that, besides providing a controlled environment in terms of overshoot temperature, also led to an oxirane index of 7.05%, higher than the industrial target of 6.5%, and an iodine value of 0.08 g/100 g I_2 after 4 h. Experimental Tests 23-25 provided measurements of the apparent kinematic viscosity of the system for different values of stirring speed – this property tends to increase at higher stirring speeds and during the course of the reaction.

An important point of caution in scaling up considerations: the heat removal in the bench reactor, as indicated in our previous work, is very intense and would not be possible to replicate in larger batch reactors. The rate of heat release by the exothermal reaction is proportional to the reactor volume (so to the 3rd power of reactor size), while the heat removal is proportional to the area for heat transfer (so to the 2nd power of reactor size); as the reactor size increases, the ratio

area-to-volume decreases, so heat removal rate does not increase at the same proportion as the heat release rate.

The second scope of this work consisted of the development of a comprehensive kinetic model for this reaction system, including the undesired reactions and the mass and heat transfer effects. The main contribution of the proposed kinetic model is the inclusion of an expression for the apparent kinematic viscosity, necessary to describe the heat transfer effect, as well as the measurements of the viscosity changes during the experiment. This expression was validated by the experimental measurements of Tests 22-25. The kinetic modeling resulted in the following values of the rate constants at 70 ºC and activation energies for the main reactions: $(5.49 \pm 0.10) \times 10^{-3}$ $L^2 \cdot mol^{-2} \cdot s^{-1}$ and $(5.09 \pm 0.11) \times 10^4$ $J \cdot mol^{-1}$ for the generation of performic acid; and $(7.30 \pm 0.48) \times 10^{-2} L \cdot mol^{-1} \cdot s^{-1}$ and $(3.80 \pm 0.39) \times 10^4$ $J \cdot mol^{-1}$ for the epoxidation reaction. The results of this kinetic model were validated with temperature profiles for the experiments described in our previous study (Tests 17-22).

AUTHOR INFORMATION

Corresponding Author

*E-mail address: rgiudici@usp.br

Author Contributions

The manuscript was written through contributions of all authors. All authors have given approval to the final version of the manuscript.

ACKNOWLEDGMENT

This work has been supported by the São Paulo Research Foundation (FAPESP, grant numbers 2019/00289-7 and 15/50684-9), the Conselho Nacional de DesenvolvimentoCientífico e Tecnológico (CNPq, grant numbers 140163/2019-0 and 309444/2016-0) and the Coordenação de Aperfeiçoamento de Pessoal de Nível Superior (CAPES, finance code 001). The authors also thank Prof. Frank Quina for revising the manuscript.

ABBREVIATIONS

A	Heat transfer area (m^2)
a_V	Volumetric interfacial area (m^{-1})
a	Coefficients for the deduction of the global heat transfer coefficient equation
C_p	Heat capacity ($J \cdot g^{-1} \cdot K^{-1}$)
c	Molar concentration ($mol \cdot L^{-1}$)
D	Diameter (m)
ESO	Epoxidized soybean oil
E	Activation energy ($J \cdot mol^{-1}$)
F	Molar flow rate ($mol \cdot s^{-1}$)
f	Binary factor
H	Partition coefficient

h	Heat transfer convective coefficient ($W \cdot m^{-2} \cdot K^{-1}$)
II	Iodine index (g/100 g I_2)
J	Mass transfer molar rate per unit of volume ($mol \cdot L^{-1} \cdot s^{-1}$)
K	Equilibrium constant
k	Kinetic constant
k_T	Thermal conductivity ($W \cdot m^{-1} \cdot K^{-1}$)
M	Molar mass ($g \cdot mol^{-1}$)
m	Mass (g)
Nu	Nusselt number
N	Stirring speed (rpm)
n	Number of measurements
OI	Oxirane index (%)
OF	Objective function
PVC	Polyvinyl chloride
Pr	Prandtl number
pK_a	Logarithmic ionization constant of formic acid
p	Parameters to estimate the global heat transfer coefficient and the apparent

	kinematic viscosity
Re	Reynolds number
R	Universal gas constant ($J \cdot mol^{-1} \cdot K^{-1}$)
r	Kinetic rate ($mol \cdot L^{-1} \cdot s^{-1}$)
S	Selectivity
T	Temperature (ºC or K)
t	Time (s, min or h)
U	Global heat transfer coefficient ($W \cdot m^{-2} \cdot K^{-1}$)
VN	Viscosity number
V	Volume (L)
We	Weber number
w	Mass fraction
X	Conversion for the double bonds of soybean oil (%)
Y	Yield (%)

Greek symbol

α	Parameters to estimate the Sauter mean diameter
β	Mass transfer coefficient ($m \cdot s^{-1}$)

ΔH	Enthalpy of reaction ($J \cdot mol^{-1}$)
μ	Dynamic viscosity ($Pa \cdot s$)
v	Apparent kinematic viscosity of the reaction system ($m^2 \cdot s^{-1}$)
ρ	Density ($g \cdot L^{-1}$)
σ	Interfacial tension ($N \cdot m$)
ϕ	Holdup

Subscripts and superscripts

aq	Aqueous phase
b	Bath
c	Continuous phase
DB	Double bonds of soybean oil
d	Dispersed phase
dec	Decantation period
EG	Epoxy group of epoxidized soybean oil
eq	Equilibrium
exp	Experimental value
ext	External (bath) conditions

FAS	Formic acid solution
FA	Formic acid
H^+	Protons from formic acid
HPS	Hydrogen peroxide solution
HP	Hydrogen peroxide
I_2	Iodine molecule
I	Impeller
i	Index for the components
int	Internal (reactor) conditions
j	Index for the phases
max	Maximum value
mod	Value determined by the model
O	Oxygen atom
org	Organic phase
PFA	Performic acid
q	Index for the reaction
r	Reference value

t	Theoretical
W	Water
w	Wall conditions
0	Initial value
32	Index for the Sauter mean diameter

REFERENCES

(1) Stolp, L. J.; Gronlund, P. J.; Kodali, D. R. Soybean Oil Fatty Acid Ester Estolides as Potential Plasticizers. *JAOCS, J. Am. Oil Chem. Soc.* **2019**, *96*, 727–738.

(2) Barcena, H.; Tuachi, A.; Zhang, Y. Teaching Green Chemistry with Epoxidized Soybean Oil. *J. Chem. Educ.* **2017**, *94*, 1314–1318.

(3) Lee, S.; Park, M. S.; Shin, J.; Kim, Y. W. Effect of the Individual and Combined Use of Cardanol-Based Plasticizers and Epoxidized Soybean Oil on the Properties of PVC. *Polym. Degrad. Stab.* **2018**, *147*, 1–11.

(4) Benecke, H. P.; Vijayendran, B. R.; Elhard, J. D. Plasticizers Derived from Vegetable Oils. US6797753B2, September 28, 2004.

(5) De Quadros Jr., J. V.; De Carvalho, J. A. Plasticized PVC Composition. US8623947B2, January 7, 2014.

(6) He, W.; Zhu, G.; Gao, Y.; Wu, H.; Fang, Z.; Guo, K. Green Plasticizers Derived from Epoxidized Soybean Oil for Poly (Vinyl Chloride): Continuous Synthesis and Evaluation in PVC Films. *Chem. Eng. J.* **2020**, *380*, 122532.

(7) Kong, J.; Han, C.; Yu, Y.; Dong, L. Production and Characterization of Sustainable Poly(Lactic Acid)/Functionalized-Eggshell Composites Plasticized by Epoxidized Soybean Oil. *J. Mater. Sci.* **2018**, *53*, 14386–14397.

(8) Ciannamea, E. M.; Ruseckaite, R. A. Pressure Sensitive Adhesives Based on Epoxidized Soybean Oil: Correlation Between Curing Conditions and Rheological Properties. *JAOCS, J. Am. Oil Chem. Soc.* **2018**, *95*, 525–532.

(9) Lee, T. H.; Park, Y. Il; Lee, S. H.; Shin, J.; Noh, S. M.; Kim, J. C. A Crack Repair Patch Based on Acrylated Epoxidized Soybean Oil. *Appl. Surf. Sci.* **2019**, *476*, 276–282.

(10) Xu, X.; Dong, F.; Yang, X.; Liu, H.; Guo, L.; Qian, Y.; Wang, A.; Wang, S.; Luo, J. Preparation and Characterization of Cellulose Grafted with Epoxidized Soybean Oil Aerogels for Oil-Absorbing Materials. *J. Agric. Food Chem.* **2019**, *67*, 637–643.

(11) Corma Canos, A.; Iborra, S.; Velty, A. Chemical Routes for the Transformation of Biomass into Chemicals. *Chem. Rev.* **2007**, *107*, 2411–2502.

(12) Campanella, A.; Baltanás, M. A. Degradation of the Oxirane Ring of Epoxidized Vegetable Oils with Hydrogen Peroxide Using an Ion Exchange Resin. *Catal. Today* **2005**, *107–108*, 208–214.

(13) Vianello, C.; Salzano, E.; Maschio, G. Thermal Behaviour of Peracetic Acid for the Epoxydation of Vegetable Oils in the Presence of Catalyst. *Process Saf. Environ. Prot.* **2018**, *116*, 718–726.

(14) De Filippis, P.; Scarsella, M.; Verdone, N. Peroxyformic Acid Formation: A Kinetic Study. *Ind. Eng. Chem. Res.* **2009**, *48*, 1372–1383.

(15) Sun, X.; Zhao, X.; Du, W.; Liu, D. Kinetics of Formic Acid-Autocatalyzed Preparation of Performic Acid in Aqueous Phase. *Chinese J. Chem. Eng.* **2011**, *19*, 964–971.

(16) Leveneur, S.; Thönes, M.; Hébert, J. P.; Taouk, B.; Salmi, T. From Kinetic Study to Thermal Safety Assessment: Application to Peroxyformic Acid Synthesis. *Ind. Eng. Chem. Res.* **2012**, *51*, 13999–14007.

(17) Santacesaria, E.; Tesser, R.; Serio, M. Di; Russo, V.; Turco, R. A New Simple Microchannel Device to Test Process Intensification. *Ind. Eng. Chem. Res.* **2011**, *50*, 2569–2575.

(18) Di Serio, M.; Russo, V.; Santacesaria, E.; Tesser, R.; Turco, R.; Vitiello, R. Liquid-Liquid-Solid Model for the Epoxidation of Soybean Oil Catalyzed by Amberlyst-16. *Ind. Eng. Chem. Res.* **2017**, *56*, 12963–12971.

(19) Campanella, A.; Baltanás, M. A. Degradation of the Oxirane Ring of Epoxidized Vegetable Oils in Liquid-Liquid Systems: I. Hydrolysis and Attack by H2O2. *Lat. Am. Appl. Res.* **2005**, *35*, 205–210.

(20) Campanella, A.; Baltanás, M. A. Degradation of the Oxirane Ring of Epoxidized Vegetable Oils in Liquid-Liquid Systems: II. Reactivity with Solvated Acetic and Peracetic Acids. *Lat. Am. Appl. Res.* **2005**, *35*, 211–216.

(21) Campanella, A.; Baltanás, M. A. Degradation of the Oxirane Ring of Epoxidized Vegetable Oils in Liquid-Liquid Heterogeneous Reaction Systems. *Chem. Eng. J.* **2006**, *118*, 141–152.

(22) Cai, X.; Zheng, J. L.; Aguilera, A. F.; Vernières-Hassimi, L.; Tolvanen, P.; Salmi, T.;

Leveneur, S. Influence of Ring-Opening Reactions on the Kinetics of Cottonseed Oil Epoxidation. *Int. J. Chem. Kinet.* **2018**, *50*, 726–741.

(23) Wisniak, J.; Navarrete, E. Epoxidation Of Fish Oil Kinetic and Optimization Model. *Ind. Eng. Chem. Prod. Res. Dev.* **1970**, *9*, 33–41.

(24) Chou, T. C.; Chang, J. Y. Acetic Acid as an Oxygen Carrier Between Two Phases for Epdxidation of Oleic Acid. *Chem. Eng. Commun.* **1986**, *41*, 253–266.

(25) Rangarajan, B.; Havey, A.; Grulke, E. A.; Culnan, P. D. Kinetic Parameters of a Two-Phase Model for in Situ Epoxidation of Soybean Oil. *J. Am. Oil Chem. Soc.* **1995**, *72*, 1161–1169.

(26) Santacesaria, E.; Tesser, R.; Di Serio, M.; Turco, R.; Russo, V.; Verde, D. A Biphasic Model Describing Soybean Oil Epoxidation with H2O2 in a Fed-Batch Reactor. *Chem. Eng. J.* **2011**, *173*, 198–209.

(27) Wu, Z.; Nie, Y.; Chen, W.; Wu, L.; Chen, P.; Lu, M.; Yu, F.; Ji, J. Mass Transfer and Reaction Kinetics of Soybean Oil Epoxidation in a Formic Acid-Autocatalyzed Reaction System. *Can. J. Chem. Eng.* **2016**, *94*, 1576–1582.

(28) Casson Moreno, V.; Russo, V.; Tesser, R.; Di Serio, M.; Salzano, E. Thermal Risk in Semi-Batch Reactors: The Epoxidation of Soybean Oil. *Process Saf. Environ. Prot.* **2017**, *109*, 529–537.

(29) Wu, Z.; Fang, J.; Xie, Q.; Zheng, T.; Wu, L.; Lu, M.; Zhang, L.; Nie, Y.; Ji, J. Macroscopic Kinetics Modelling of Liquid–Liquid Reaction System: Epoxidation of Fatty Acid Methyl Esters. *Ind. Crops Prod.* **2018**, *122*, 266–276.

(30) Cai, C.; Dai, H.; Chen, R.; Su, C.; Xu, X.; Zhang, S.; Yang, L. Studies on the Kinetics of in Situ Epoxidation of Vegetable Oils. *Eur. J. Lipid Sci. Technol.* **2008**, *110*, 341–346.

(31) Zheng, J. L.; Wärnå, J.; Salmi, T.; Burel, F.; Taouk, B.; Leveneur, S. Kinetic Modeling Strategy for an Exothermic Multiphase Reactor System: Application to Vegetable Oils Epoxidation Using Prileschajew Method. *AIChE J.* **2016**, *62*, 726–741.

(32) Chen, C.; Cai, L.; Li, L.; Bao, L.; Lin, Z.; Wu, G. Heterogeneous and Non-Acid Process for Production of Epoxidized Soybean Oil from Soybean Oil Using Hydrogen Peroxide as Clean Oxidant over TS-1 Catalysts. *Microporous Mesoporous Mater.* **2019**, *276*, 89–97.

(33) Bhalerao, M. S.; Kulkarni, V. M.; Patwardhan, A. V. Ultrasound-Assisted Chemoenzymatic Epoxidation of Soybean Oil by Using Lipase as Biocatalyst. *Ultrason. Sonochem.* **2018**, *40*, 912–920.

(34) Zou, X.; Nie, X.; Tan, Z.; Shi, K.; Wang, C.; Wang, Y.; Zhao, X. Synthesis of Sulfonic Acid-Functionalized Zirconium Poly(Styrene-Phenylvinyl-Phosphonate)-Phosphate for Heterogeneous Epoxidation of Soybean Oil. *Catalysts*. **2019**, *9*, 710-721.

(35) Turco, R.; Pischetola, C.; Di Serio, M.; Vitiello, R.; Tesser, R.; Santacesaria, E. Selective Epoxidation of Soybean Oil in the Presence of H-Y Zeolite. *Ind. Eng. Chem. Res.* **2017**, *56*, 7930–7936.

(36) Aguilera, A. F.; Tolvanen, P.; Wärnå, J.; Leveneur, S.; Salmi, T. Kinetics and Reactor Modelling of Fatty Acid Epoxidation in the Presence of Heterogeneous Catalyst. *Chem. Eng. J.* **2019**, *375*, 121936.

(37) Kerr, J. A. Bond Dissociation Energies by Kinetic Methods. *Chem. Rev.* **1966**, *66*, 465–

500.

(38) Rakotondramaro, H.; Wärnå, J.; Estel, L.; Salmi, T.; Leveneur, S. Cooling and Stirring Failure for Semi-Batch Reactor: Application to Exothermic Reactions in Multiphase Reactor. *J. Loss Prev. Process Ind.* **2016**, *43*, 147–157.

(39) Leveneur, S.; Zheng, J.; Taouk, B.; Burel, F.; Wärnå, J.; Salmi, T. Interaction of Thermal and Kinetic Parameters for a Liquid-Liquid Reaction System: Application to Vegetable Oils Epoxidation by Peroxycarboxylic Acid. *J. Taiwan Inst. Chem. Eng.* **2014**, *45*, 1449–1458.

(40) Leveneur, S.; Pinchard, M.; Rimbault, A.; Safdari Shadloo, M.; Meyer, T. Parameters Affecting Thermal Risk through a Kinetic Model under Adiabatic Condition: Application to Liquid-Liquid Reaction System. *Thermochim. Acta* **2018**, *666*, 10–17.

(41) Leveneur, S. Thermal Safety Assessment through the Concept of Structure-Reactivity: Application to Vegetable Oil Valorization. *Org. Process Res. Dev.* **2017**, *21*, 543–550.

(42) Vianello, C.; Piccolo, D.; Lorenzetti, A.; Salzano, E.; Maschio, G. Study of Soybean Oil Epoxidation: Effects of Sulfuric Acid and the Mixing Program. *Ind. Eng. Chem. Res.* **2018**, *57*, 11517–11525.

(43) Cortese, B.; De Croon, M. H. J. M.; Hessel, V. High-Temperature Epoxidation of Soybean Oil in Flow-Speeding up Elemental Reactions Wanted and Unwanted. *Ind. Eng. Chem. Res.* **2012**, *51*, 1680–1689.

(44) de Quadros, J. V.; Giudici, R. Epoxidation of Soybean Oil at Maximum Heat Removal and Single Addition of All Reactants. *Chem. Eng. Process. Process Intensif.* **2016**, *100*,

87–93.

(45) Esteban, B.; Riba, J.-R.; Baquero, G.; Rius, A.; Puig, R. Temperature Dependence of Density and Viscosity of Vegetable Oils. *Biomass and Bioenergy* **2012**, *42*, 164–171.

(46) Campanella, A.; Fontanini, C.; Baltanás, M. A. High Yield Epoxidation of Fatty Acid Methyl Esters with Performic Acid Generated in Situ. *Chem. Eng. J.* **2008**, *144*, 466–475.

(47) Santacesaria, E.; Renken, A.; Russo, V.; Turco, R.; Tesser, R.; Di Serio, M. Biphasic Model Describing Soybean Oil Epoxidation with H 2O 2 in Continuous Reactors. *Ind. Eng. Chem. Res.* **2012**, *51*, 8760–8767.

(48) Kim, M. H.; Kim, C. S.; Lee, H. W.; Kim, K. Temperature Dependence of Dissociation Constants for Formic Acid and 2,6-Dinitrophenol in Aqueous Solutions up to 175°C. *J. Chem. Soc. - Faraday Trans.* **1996**, *92*, 4951–4956.

(49) Whitman, W. G. Preliminary Experimental Confirmation of the Two-Film Theory of Gas Absorption. *Chem. Met. Eng.* **1923**, *29*, 146.

(50) Khakpay, A.; Abolghasemi, H.; Salimi-Khorshidi, A. The Effects of a Surfactant on Mean Drop Size in a Mixer-Settler Extractor. *Chem. Eng. Process. Process Intensif.* **2009**, *48*, 1105–1111.

(51) Ullmann's. *Encyclopedia of Industrial Chemistry*, 7th ed.; VCH: Weinheim, 2011.

(52) Easton, M. F.; Mitchell, A. G.; Wynne-Jones, W. F. K. The Behaviour of Mixtures of Hydrogen Peroxide and Water. *Lamp* **1952**, *1*, 796–801.

(53) Smith, J. M.; Van Ness, H. C.; Abbott, M. M. *Introduction to Chemical Engineering*

Thermodynamics, 8th ed.; McGraw-Hill: New York, 2018.

(54) de Guzman, J. Relation between Fluidity and Heat of Fusion. *An. la Soc. Española Física y Química* **1913**, *11*, 353–362.

(55) Santacesaria, E.; Russo, V.; Tesser, R.; Turco, R.; Di Serio, M. Kinetics of Performic Acid Synthesis and Decomposition. *Ind. Eng. Chem. Res.* **2017**, *56*, 12940–12952.

(56) Blanksby, S. J.; Ellison, G. B. Bond Dissociation Energies of Organic Molecules. *Acc. Chem. Res.* **2003**, *36*, 255–263.

(57) Akse, H.; Beek, W. J.; van Berkel, F. C. A. A.; de Graauw, J. The Local Heat Transfer at the Wall of a Large Vessel Agitated by Turbine Impellers. *Chem. Eng. Sci.* **1967**, *22*, 135–146.

Appendix A. Derivation of equation (41)

The overall heat transfer coefficient between the reaction medium inside the reactor and the water in the thermostatic bath is:

$$\frac{1}{U} = \frac{1}{h_{\text{int}}} + \frac{D_{\text{w}}}{k_{T,\text{w}}} + \frac{1}{h_{\text{ext}}} \qquad \text{(A1)}$$

in which h_{int} is the heat transfer coefficient between the reactor wall and the reaction medium, h_{ext} is the heat transfer coefficient between the reactor wall and the fluid in the thermostatic bath, and d_w and $k_{T,w}$ are, respectively, the thickness and the thermal conductivity of the reactor wall.

Considering that the stirring condition on the bath side and the thermal resistance to heat conduction through the wall are constant:

$$\frac{1}{U} = \frac{1}{h_{int}} + p_2 \qquad \text{(A2)}$$

The heat transfer on the reactor side is usually expressed via a correlation of dimensionless groups (*Nu*, *Re*, and *Pr*, respectively, the Nusselt number, the Reynolds number and the Prandtl number):

$$Nu = a_1 (Re)^{a_2} (Pr)^{a_3} \left(\frac{\mu}{\mu_w}\right)^{a_4} \qquad \text{(A3)}$$

or

$$\left(\frac{h_{int} D_I}{k_T}\right) = a_1 \left(\frac{D^2 N \rho}{\mu}\right)^{a_2} \left(\frac{C_p \mu}{k_T}\right)^{a_3} \left(\frac{\mu}{\mu_w}\right)^{a_4} \qquad \text{(A4)}$$

in which D_I is the diameter of the stirrer, D is the diameter of the reactor, N is the rotation speed of the stirrer, ρ, C_p , k_T and μ are, respectively, the density, specific heat, thermal conductivity,

and viscosity of the fluid (reaction mixture), μ_w is the viscosity of the fluid at the wall temperature, and a_1, a_2, a_3 and a_4 are empirical parameters.

For Newtonian fluids, $a_2 \cong 2/3$, $a_3 \cong 1/3$ and $a_4 \cong 1/7$ [57] and, assuming that $(\mu/\mu_w) \cong$ constant and a fixed reactor/stirrer geometry:

$$h_{int} = a_5 (k_T)^{2/3} (C_p)^{1/3} (\rho)^{2/3} (\mu)^{-1/3} (N)^{2/3} \quad \text{(A5)}$$

Substituting in equation (A2) results:

$$\frac{1}{U} = \frac{1}{a_5 (k_T)^{2/3} (C_p)^{1/3} (\rho)^{2/3} (\mu)^{-1/3} (N)^{2/3}} + p_2 \quad \text{(A6)}$$

Among the physical properties present in this equation, a sensitivity analysis shows that viscosity is the most influential one, so:

$$U = 1/(p_1 v^{1/3} N^{-2/3} + p_2) \quad \text{(A7)}$$

==========

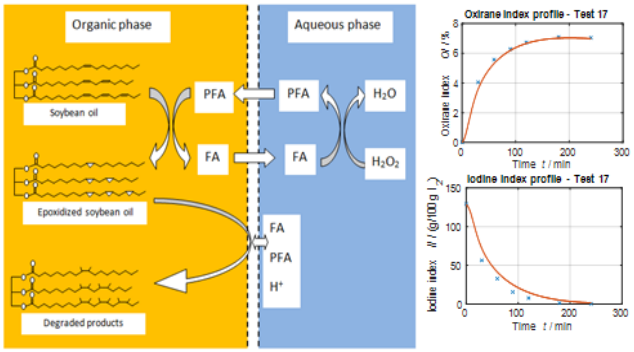

(For Table of Contents use only)